Neurobiology of Disease

Differential Activation of Pain Circuitry Neuron Populations in a Mouse Model of Spinal Cord Injury-Induced Neuropathic Pain

Eric V. Brown, Ayma F. Malik, Elizabeth R. Moese, Abigail F. McElroy, and Angelo C. Lepore
Department of Neuroscience, Vickie and Jack Farber Institute for Neuroscience, Sidney Kimmel Medical College at Thomas Jefferson University, Philadelphia, Pennsylvania 19107

Neuropathic pain (NP) is one of the most common and debilitating comorbidities of spinal cord injury (SCI). Current therapies are often ineffective due in part to an incomplete understanding of underlying pathogenic mechanisms. In particular, it remains unclear how SCI leads to dysfunction in the excitability of nociceptive circuitry. The immediate early gene c-Fos has long been used in pain processing locations as a marker of neuronal activation. We employed a mouse reporter line with fos-promoter driven Cre-recombinase to define neuronal activity changes in relevant pain circuitry locations following cervical spinal cord level (C)5/6 contusion (using both females and males), a SCI model that results in multiple forms of persistent NP-related behavior. SCI significantly increased activation of cervical dorsal horn (DH) projection neurons, as well as induced a selective reduction in the activation of a specific DH projection neuron subpopulation that innervates the periaqueductal gray (PAG), an important brain region involved in descending inhibitory modulation of DH pain transmission. SCI also increased the activation of both protein kinase C (PKC)γ and calretinin excitatory DH interneuron populations. Interestingly, SCI promoted a significant decrease in the activation selectively of neuronal nitric oxide synthase (nNOS)-expressing inhibitory interneurons of cervical DH. In addition, SCI altered activation of various supraspinal neuron populations associated with pain processing, including a large increase in thalamus and a significant decrease in PAG. These findings reveal a complex and diverse set of SCI-induced neuron activity changes across the pain circuitry neuraxis. Moving forward, these results can be used to inform therapeutic targeting of defined neuronal populations in NP.

Key words: **dorsal horn; fos; interneuron; neuropathic pain; spinal cord injury; TRAP**

Significance Statement

Neuropathic pain (NP) is one of the most common and highly debilitating comorbidities of spinal cord injury (SCI). Unfortunately, current therapies are often ineffective due in part to an incomplete understanding of underlying pathogenic mechanisms. In particular, it remains unclear how SCI leads to dysfunction in excitability of nociceptive circuitry. Using a FosTRAP2 reporter mouse line in a model of SCI-induced NP, we show SCI alters activation of a number of important interneuron and projection neuron populations across relevant spinal cord and brain locations of the pain circuitry neuraxis. These data suggest a role for maladaptive plasticity involving specific subpopulations of neurons and circuits in driving SCI-induced chronic pain. Moving forward, these results can be used to inform therapeutic targeting of defined neuronal populations in NP.

Introduction

Chronic neuropathic pain (NP) is one of the most common comorbidities of spinal cord injury (SCI), affecting as many as 80% of patients (Finnerup et al., 2001). It can manifest as allodynia, in which previously innocuous sensory stimuli become painful, and can therefore disrupt many activities of daily living and have debilitating effects on quality of life (Siddall et al., 2003). SCI-induced NP can also involve hyperalgesia, in which there is enhanced sensitivity to a normally-noxious stimulus. In addition, a large portion of individuals with SCI experience spontaneous pain in the absence of peripheral stimulation. Moreover, current

Received Aug. 4, 2021; revised Feb. 3, 2022; accepted Feb. 7, 2022.

Author contributions: E.V.B. and A.C.L. designed research; E.V.B., A.F.M., E.R.M., and A.F.M. performed research; E.V.B., A.F.M., E.R.M., and A.F.M. analyzed data; E.V.B. wrote the first draft of the paper; E.V.B. and A.C.L. edited the paper; E.V.B. and A.C.L. wrote the paper.

This work was supported by the National Institute of Neurological Disorders and Stroke Grant R01NS110385 (to A.C.L.).

The authors declare no competing financial interests.

Correspondence should be addressed to Angelo C. Lepore at angelo.lepore@jefferson.edu.

https://doi.org/10.1523/JNEUROSCI.1596-21.2022

therapeutics have limited efficacy, due in part to an incomplete understanding of the mechanisms underlying this type of pathologic pain (Cardenas and Jensen, 2006). There is therefore an urgent need to more clearly define SCI-induced changes in sensory processing to begin to develop more effective therapeutics for affected individuals.

Spinal cord dorsal horn (DH) receives innervation by primary sensory afferents and is critical for the processing of nociceptive sensory information (Todd, 2010). Highly heterogeneous and complex microcircuits of excitatory and inhibitory interneurons integrate somatosensory nociceptive information and gate signaling to supraspinal pain relevant nuclei (Mendell, 2014; Todd, 2017). Genetic and pharmacologic manipulation (and/or ablation) of DH neurons has helped to define roles of specific subpopulations of DH interneurons and projection neurons in normal pain processing (Choi et al., 2020; Sheahan et al., 2020). Furthermore, injury induced changes in DH neuron signaling have been implicated in models of NP, in particular peripheral nerve injury. While SCI induces reactivity of glial populations in DH such as microglia and astrocytes that has been therapeutically targeted to prevent and/or reverse NP (Gwak et al., 2012), relatively little is known about SCI-induced changes to the activation state of specific DH neuron microcircuits.

Inhibitory interneurons in DH provide both presynaptic and postsynaptic inhibition of primary afferents, excitatory interneurons, and second-order pain projection neurons and are critically important for normal somatosensory processing. There are four major populations of inhibitory interneurons located primarily in Laminae II/III, which are neurochemically defined by expression of neuronal nitric oxide synthase (nNOS), parvalbumin, neuropeptide Y (NPY), or galanin/dynorphin (Polgár et al., 2013). Several of these populations have established roles in nociception. For example, $nNOS^+$ interneurons inhibit cutaneous mechanical signaling via synapses with protein kinase C (PKC) γ^+ excitatory interneurons, as well as by directly inhibiting Lamina I spinal projection neurons (Puskár et al., 2001; Sardella et al., 2011). Activation of $nNOS^+$ interneurons decreases pain-like responses to both mechanical and thermal stimuli (Huang et al., 2018). Additionally, NPY^+ neurons provide direct inhibition of DH projection neuron signaling, and following peripheral nerve injury activity of NPY^+ interneurons is decreased, leading to mechanical allodynia (Cameron et al., 2015; Iwagaki et al., 2016; Tashima et al., 2021). There is an overall loss of DH inhibitory signaling (as measured by decreased GABA/GAD expression), which plays a role in models of peripheral nerve injury and SCI-induced NP (Ibuki et al., 1997; Drew et al., 2004; Kami et al., 2016). Increased activity of excitatory interneurons has also been implicated in underlying pathologic pain in preclinical models. For example, loss of parvalbumin input to PKC γ^+ excitatory interneurons partially underlies mechanical allodynia in a model of peripheral nerve injury (Petitjean et al., 2015). Importantly, it remains unclear how activity of specific subpopulations of inhibitory and excitatory interneurons contributes to the generation and persistence of SCI-induced NP.

After processing by DH interneurons, somatosensory information is passed by DH projection neurons to supraspinal pain processing areas. DH projection neurons are large diameter neurons characterized, at least in a subset of the population, by their expression of the neurokinin-1 receptor (NK1R). They form a band in Lamina I, with smaller numbers spread throughout Laminae III–VIII and the lateral spinal nucleus (Todd, 2010; Wercberger and Basbaum, 2019). They receive ~50% of their glutamatergic input from primary afferents, but their activity is significantly regulated by DH interneurons (Polgár et al., 2010a; Todd, 2010). Projection neurons of the DH innervate several supraspinal nuclei, which function together to shape the stimulus induced pain experience. The ventroposterolateral (VPL) nucleus of the thalamus, the canonical site of pain processing, receives only a small fraction of DH projections, with the majority synapsing in one or more of several other brain nuclei that each regulates specific aspects of the pain response (Spike et al., 2003; Polgár et al., 2010b). For example, the lateral parabrachial nucleus (LPB) regulates pain induced affectual changes, while the periaqueductal gray (PAG) coordinates top-down modulation of DH neuronal signaling indirectly through projections to the dorsal raphe (DR) and locus coeruleus (LC) and directly via descending projections to the spinal cord DH (Heinricher et al., 2009). As a population, DH projection neurons synapse in multiple supraspinal locations, and it remains unknown whether SCI alters activation of specific subpopulations of projection neurons that innervate select supraspinal nuclei (Al-Khater and Todd, 2009).

Immediate early genes, which are transcribed in the absence of *de novo* protein synthesis in response to neural stimulation, have been used as markers of neuronal activation (Herschman, 1991). In the context of nociception, the transcription factor c-Fos has long been used in DH as an immediate early gene marker of neuronal activation (Hunt et al., 1987; Menétrey et al., 1989). Recently, a mouse line has been developed that expresses a *fos*-promoter driven, estrogen-dependent Cre-recombinase (FosTRAP2; DeNardo et al., 2019). Tamoxifen administration to these mice induces recombination and therefore permanent expression of Cre-dependent genes in Fos-expressing neurons (Guenthner et al., 2013; DeNardo et al., 2019). We crossed these targeted recombination in active populations 2 (TRAP2) mice with a genetic Cre-regulated TdTomato reporter animal [or through targeted intraspinal viral delivery of Cre-dependent green fluorescent protein (GFP) to the DH] to clearly visualize Fos-expressing activated neurons in the context of SCI, both in the presence or absence of different peripheral sensory stimulus modalities.

Using TRAP2 mice, we delivered a clinically relevant cervical hemi-contusion SCI, which we have previously reported induces multiple forms of persistent at-level and below-level NP-related behaviors, including mechanical allodynia and thermal hyperalgesia consistently in all injured mice (Putatunda et al., 2014; Watson et al., 2014; Ritter et al., 2015; Falnikar et al., 2016; Heinsinger et al., 2020; Brown et al., 2021). We used this paradigm to explore SCI-induced activation changes in three neuronal population groups relevant to pain processing: interneurons of the cervical DH and lumbar DH, DH projection neurons of the cervical spinal cord, and neurons in several pain-relevant supraspinal areas (including those that receive direct projections from DH). We quantified FosTRAP2 reporter levels as a marker of neuronal activity in these populations at multiple time points postinjury, as well as in response to mechanical or thermal sensory stimulation paradigms that evoke NP-like behavioral responses in SCI animals.

Materials and Methods

Animals

Animal procedures were approved by Thomas Jefferson University's Institutional Animal Care and Use Committee (IACUC) and were

conducted in compliance with the National Institutes of Health (NIH) *Guide for the Care and Use of Laboratory Animals* and the ARRIVE (Animal Research: Reporting of In Vivo Experiments) guidelines. Mouse lines Fos2A-iCreER (TRAP2; stock #030323) and Ai14 (stock #007908) were obtained from The Jackson Laboratory. Mouse lines were maintained separately as homozygotes, and cross bred for experiments. F1 generation of TRAP2 mice crossed with Ai14 mice were used for most experiments, unless otherwise specified. A mix of both female and male mice was used between 20 and 30 g, with an *n* of three to eight animals per group for the various analyses.

SCI surgeries

TRAP2 x Ai14 mice were anesthetized with 1% isoflurane. Contusion SCI was conducted, as previously described (Brown, Falnikar et al., 2021). Briefly, an incision was made from just caudal to the skull to just rostral to the T1 process and muscle layers were separated individually, exposing the dorsal laminae of the spinal column. The right side of the dorsal laminae above the cervical spinal cord level (C)5 and C6 spinal cord were removed using rongeurs. The Infinite Horizons spinal impactor (Precision Systems and Instrumentation) was used to generate a contusion SCI on the right side of the C5/6 spinal cord using the following parameters: 0.7-mm impactor tip, 50 kdynes of force, 2 s of dwell time. Laminectomy-only uninjured controls received identical surgeries but did not receive a contusion. While we do not present in the current study functional data from these cervical contusion SCI mice showing the effects of the injury on various NP-related behaviors, we have repeatedly demonstrated that this exact same mouse unilateral C5/6 contusion model reproducibly produces at-level (in the forepaw plantar surface) thermal hyperalgesia and mechanical allodynia in every mouse tested (Heinsinger et al., 2020; Brown, Falnikar et al., 2021). In addition, these NP-related thermal and mechanical phenotypes persist in every mouse until chronic time points postinjury. Furthermore, the thermal and mechanical phenotypes exhibited by these cervical contusion mice show an extremely low amount of animal-to-animal variability. Therefore, because every mouse subjected to this SCI paradigm exhibits robust thermal hyperalgesia and mechanical allodynia and also because these sensory behavioral phenotypes show very little variability across animals, we were unable to perform a within-animal correlation of the degree of FosTRAP2 labeling (to identify putatively activated neurons) and the degree of NP-like behavior exhibited by that same animal.

Tamoxifen administration and peripheral stimulation paradigms

Tamoxifen (MilliporeSigma) was dissolved to a concentration of 1 mg/10 µl and was delivered via intraperitoneal injection with an insulin syringe 1× per day for 2 d (160 µg/g bodyweight). Our SCI paradigm causes mechanical allodynia (decreased paw withdrawal threshold in response to a previously innocuous mechanical stimulus; Heinsinger et al., 2020; Brown et al., 2021). Ipsilateral forepaw withdrawal threshold for intact and laminectomy-only mice is ~1.5 g of force using von Frey filaments, while the paw withdrawal threshold of cervical contusion SCI mice is ~0.1 g (Heinsinger et al., 2020; Brown et al., 2021). We were therefore able to design a paradigm in which we could stimulate the ipsilateral forepaw of animals in a way which would be nocifensive to SCI animals but not laminectomy mice. Immediately before tamoxifen administration, animals were scruffed and a von Frey filament (Aesthesio Precision Tactile Evaluator, DanMic Global) applying 0.16 g of force was applied 10 times to the plantar surface of the ipsilateral forepaw. Care was used to ensure applications were made to the center of the forepaw, avoiding the toe pads, and applications were considered complete as soon as the filament was bent and force was applied (there was no dwell time; the filament was touched to the surface of the forepaw, bent, and then immediately removed). In one experiment, uninjured laminectomy-only animals were instead stimulated using a 1-g filament. The thermal stimulation paradigm was designed in a similar fashion. As measured with a Hargeaves apparatus (Ugo Basile), the latency to ipsilateral forepaw withdrawal of uninjured laminectomy-only mice is ~20 s. Following cervical contusion SCI, the forepaw withdrawal threshold decreases to ~10 s (Heinsinger et al., 2020; Brown et al., 2021). Therefore, in similar fashion to applying the mechanical stimulus, we applied a 10 s thermal stimulus to the plantar surface of the ipsilateral forepaw in conjunction with tamoxifen injection. While we did not perform quantitative von Frey or Hargreaves testing on the FosTRAP2 mice used for histologic analyses in this study, we nevertheless did observe that all paw-stimulated mice exhibited the typical expected behavioral phenotypes that we consistently observe for mice subjected to this SCI paradigm, including supraspinal-associated behaviors in response to each thermal and mechanical stimulation such as guarding, licking, vocalization, and escape behaviors.

Viral injections

Following hemi-laminectomies above the ipsilateral C7/C8 spinal cord, an AAV1 pCAG-FLEX-EGFP-WPRE (addgene: 51502-AAV1) was injected into the DH using a UltraMicroPump and Micro4 Microsyringe Pump Controller (World Precision Instruments; 0.2 mm deep, 1 mm lateral to the spinal midline; 1 µl per injection site, injected over 5 min; Lepore, 2011; Li et al., 2015a; Falnikar et al., 2016). Injection was delivered using a pulled glass pipette attached with silicone to a 10-µl Hamilton syringe (Hamilton, catalog #1701). The needle was moved into position and allowed to rest for 5 min before the injection, and 5 min after injection, before being removed from the spinal cord. Biobrane (Smith&Nephew) was gently placed over the spinal cord at the two injection sites before wound closure. At one week after injection, a second surgery was conducted in which animals were given either laminectomy-only surgery or C5/6 contusion (ipsilateral to the injection sites), as described above. This vector does not have a constitutive reporter to detect all transduced cells (regardless of their activation state). Instead, the fluorescent reporter is only observed in activated neurons.

Tissue processing

Animals were killed using an overdose of ketamine (100 mg/kg) and xylazine (5 mg/kg), then transcardially perfused with 0.9% saline, followed by 4% paraformaldehyde. Spinal cord and brain were dissected and placed in 4% PFA overnight, then transferred to 0.1 M phosphate buffer for 24 h, before being placed in 30% sucrose for at least 3 d before cryosectioning. Spinal cords were flash frozen in tissue freezing media (General Data Healthcare), then sectioned transversely at a thickness of 30 μm. Similarly, brains were sectioned coronally at a thickness of 40 μm. Brains and spinal cords were mounted directly on Superfrost Plus slides. Following DH projection neuron tracing, brains of animals were sectioned at 40 µm and stored free-floating in TBS with 0.05% sodium azide, before being mounted on Superfrost slides before immunohistochemistry.

Immunohistochemistry

For immunostaining analysis, cervical spinal cord sections were located in intact tissue caudal to the contusion epicenter (corresponding to the C7/8 spinal cord level). Lesion epicenter was defined as the transverse spinal cord section with the largest percentage of lesion area (Lepore et al., 2011; Li et al., 2015b). This caudal location was chosen because it is the site of input to DH from primary sensory afferents that innervate the plantar surface of the ipsilateral forepaw. Lumbar spinal cord analysis was performed at L4/L5, as these segments receive primary afferent input from the plantar surface of the hindpaw. With the exception c-Fos, slides for immunohistochemistry were dried overnight at room temperature, then for 1 h at 37C. For inhibitory interneuron subtype markers, antigen retrieval was used. Slides were placed in a 95C water bath for 10 min in a slide holder in antigen retrieval buffer (R&D Systems, CTS015). A hydrophobic barrier was then applied around the sections to be immunostained, and slides were washed three times for 5 min each in PBS. Slides were then blocked for 1 h in blocking buffer (5% donkey serum and 0.1% Triton X-100 in PBS). Slides were then incubated at 4C overnight at the concentrations specified below in blocking buffer. Slides were then washed 3 × 5 min in PBS and incubated in the appropriate secondary antibody listed below at a concentration of 1:200 in blocking buffer before being mounted with Fluorsave (Millipore Sigma). The protocol used for c-Fos immunohistochemistry can be found published by DeNardo et al. (2019). Primary antibodies used were: rabbit anti-c-Fos (Synaptic Systems,

AB_2231974, 1:1000), goat anti-Pax2 (R&D Systems, AB_10889828, 1:250), goat anti-calretinin (R&D Systems, AB_2068516, 1:300), goat anti-PKCγ (R&D Systems, AB_2300308, 1:300), mouse anti-parvalbumin (Millipore Sigma, AB_477329, 1:1000), rabbit anti-neuropeptide-Y (Peninsula Laboratories, AB_518504, 1:500), rabbit anti-nNos (Cell Signaling, AB_2612783, 1:250), and chicken anti-GFP (Aves Labs, AB_10000240, 1:1000). Secondary antibodies from Jackson ImmunoResearch Laboratories, Inc. were used at 1:200: donkey anti-rabbit Alexa Fluor 647, AB_2492288; donkey anti-rabbit Alexa Fluor 488, AB_2313584; donkey anti-mouse Alexa Fluor 488, AB_2340846; donkey anti-goat Alexa Fluor 488, AB_2340428; and donkey anti-goat Alexa Fluor 647, AB_2340436.

Imaging and analysis

Immunohistochemistry staining was imaged using either a Zeiss Axio10 Imager or a Leica SP8 confocal microscope. Displayed images are shown as max projected z-stacks or as orthogonal projections. Co-labeling of cells for tdTomato and markers of neuronal subpopulations was confirmed in three dimensions and counted using ImageJ. Each data point is the average of three sections per animal; for NK1R analysis, each data point is the sum of five sections per animal. It was necessary to quantify NK1R staining in this fashion because of the very low number of Lamina I NK1R$^+$ projection neurons in the cervical spinal cord. Images were prepared for display using LAS X imaging software (RRID: SCR_013673) and ImageJ (RRID: SCR_003070). We performed quantification separately in Lamina I, and Laminae II/III. We defined Lamina I as the area encompassed by NK1R immunolabeling band, Lamina II as the area extending from the ventral border of NK1R immunolabeling band to the ventral border of PKCγ immunolabeling band (which is restricted to neurons of the inner region of Lamina II). Lamina III was defined from a reference atlas (Watson et al., 2009), as described previously (Polgár et al., 2005). Brain regions were defined from a reference atlas, and the average of three to five randomly selected sections were quantified for each region. ImageJ was used: to count numbers of TdTomato$^+$ cells; for injection experiments to count numbers of GFP$^+$ putative axon profiles; and to trace the total length of GFP$^+$ putative axon profiles in each section. For PAG analyses, we quantified both TdTomato and GFP expression from coronal brain sections containing PAG completely encircling the cerebral aqueduct (between atlas sections 93 and 103 in the Allen Brain Atlas). We randomly selected sections from this region for analysis as it had the highest density of GFP labeling in our intra-DH virus injection experiments. Care was chosen to closely match locations for TdTomato$^+$ cell counting and GFP$^+$ profile analysis.

Experimental design and statistical analysis

All statistical analysis was performed using GraphPad Prism (RRID: SCR_002798). Parametric one-way ANOVA with Tukey's *post hoc* test was used for all comparisons, unless otherwise specified. All data are displayed as mean ± SEM. Before starting the study, mice were randomly assigned to experimental groups, and the different surgical procedures used within a given experiment were randomly distributed across these mice (and within a given surgical day). For the various analyses, we repeated the experiment in multiple cohorts of animals. All surgical procedures and subsequent histologic analyses were conducted in a blinded manner. In Results, we provide details of sample numbers, statistical tests used and the results of all statistical analyses (including exact *p*-values, *t* values, and *F* values) for each experiment and for all statistical comparisons. We authenticated relevant experimental regents to ensure that they performed similarly across experiments and to validate the resulting data. Whenever we used a new batch of the AAV vector, we verified that the virus performed equivalently from batch-to-batch by confirming in every animal that the vector transduced neurons and induced similar expression of the GFP reporter for each batch. For all antibodies used in the immunohistochemistry studies, we always verified (when receiving a new batch from the manufacturer) that labeling in the spinal cord and brain coincided with the established expression pattern of the protein. We have provided Research Resource Identification Initiative (RRID) numbers for all relevant reagents (i.e., antibodies and computer programs) throughout Materials and Methods.

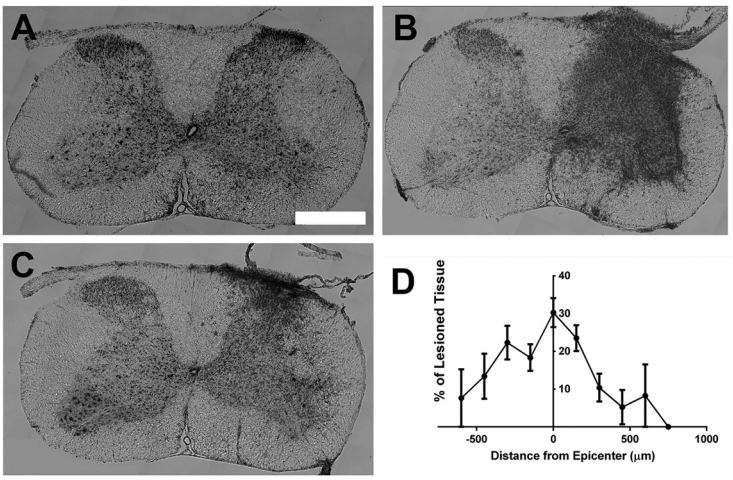

Figure 1. Lesion size quantification. Lesion size was quantified via cresyl violet staining. Representative images of intact spinal cord (***A***), lesion epicenter (***B***), and damaged spinal cord location caudal to the epicenter (***C***). Quantification of lesion size (***D***).

Results

Cervical SCI altered DH neuron activation in a lamina-specific manner

We assessed SCI-induced neuronal activation in behaviorally relevant areas of the DH in TRAP2 reporter mice. We performed a cervical level 5/6 unilateral contusion SCI or laminectomy-only control surgery and quantified the number of Fos-expressing (activated) neurons at the time when NP-related behavioral phenotypes are first established in this SCI model [14 d postinjury (dpi)] and also at a time point when these NP behaviors persist chronically (35 dpi; Heinsinger et al., 2020; Brown et al., 2021). The SCI lesion was restricted to the right side of the spinal cord, with an epicenter located between the C5 and C6 levels and with a total lesion length of ~1 mm along the rostro-caudal axis that was consistent across animals (Fig. 1; $n = 5$ mice). We first assessed the effect of SCI alone; to do this, we induced recombination in Fos positive cells via intraperitoneal tamoxifen administration at either 14 or 35 d postsurgery, and then waited 5 d before killing to allow time for adequate reporter expression. In separate groups of mice, we performed the same experiments, except contemporaneous to tamoxifen administration, we mechanically stimulated the ipsilateral forepaw using a paradigm based on our previous work (Heinsinger et al., 2020; Brown et al., 2021) that is nocifensive to cervical contusion mice, but not to uninjured laminectomy-only animals. We further explored whether results found following mechanical stimulation were sensory modality specific using a third experimental paradigm in which a thermal, rather than mechanical, stimulus was similarly applied to the ipsilateral forepaw at the time of tamoxifen administration (Fig. 2*B*, experimental timeline). For all results in this study obtained from the cervical spinal cord, we performed our TRAP2 analysis in the intact, ipsilateral C7/8 DH caudal to the contusion site (Fig. 2*A*, diagram depicting location of histologic analysis). We chose this specific DH location because it receives input from the central projections of dorsal root ganglion

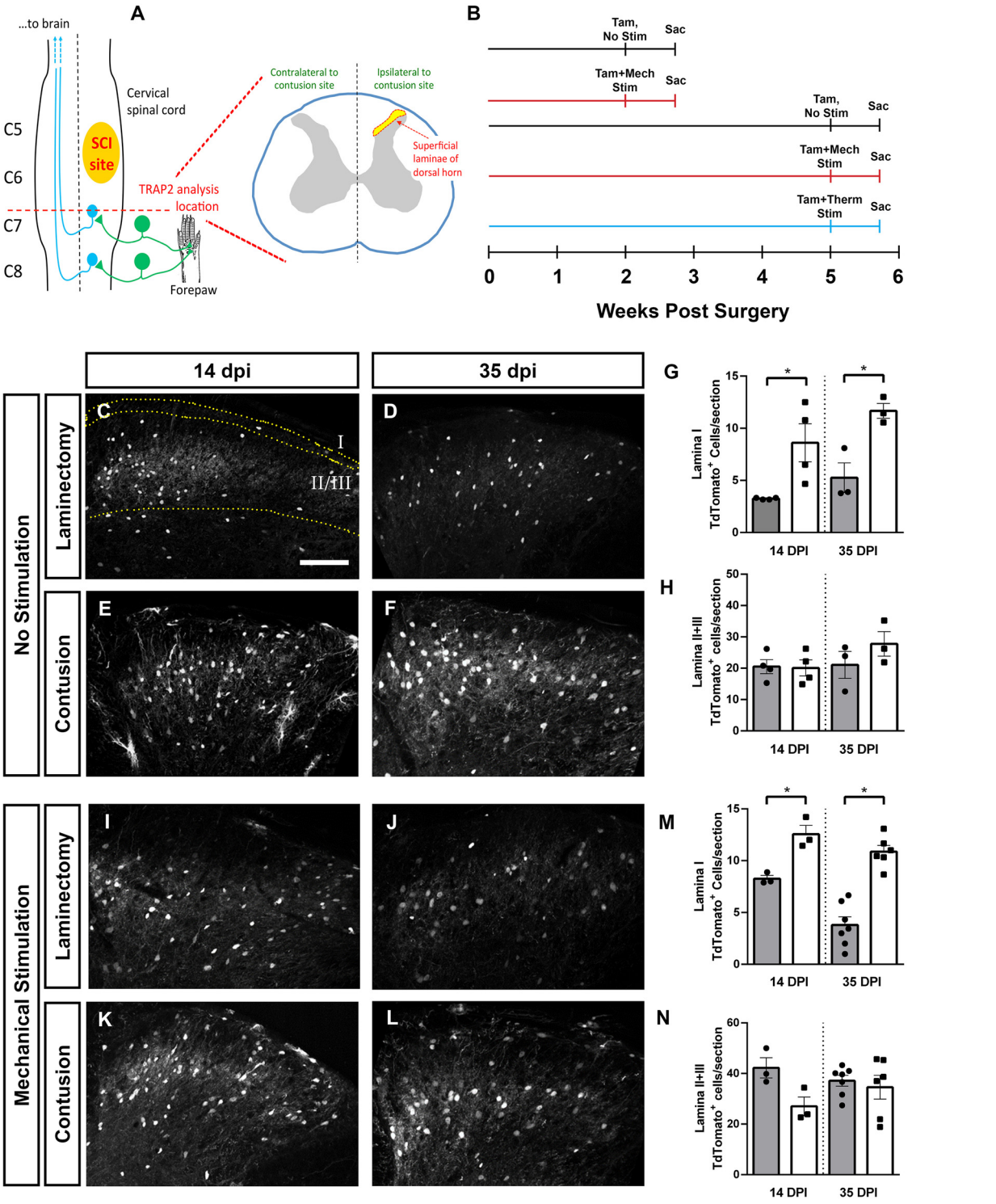

Figure 2. Cervical SCI altered DH neuron activation in a lamina-specific manner. Unilateral C5/6 contusion or C5/6 laminectomy-only control was delivered to the right side of FosTRAP2 mice, and TdTomato$^+$ cell counts were performed in the intact, ipsilateral DH at C7/8. Diagram of injury and site of analysis (***A***). Activated neurons were quantified at 14 and 35 dpi, in the absence of ipsilateral forepaw stimulation, following mechanical stimulation of the ipsilateral forepaw (at 14 or 35 dpi), or following thermal stimulation of the ipsilateral forepaw (at 35 dpi). Timeline of experiments (***B***). Representative images of the DH at 14 d (***C***) and 35 d (***D***) after laminectomy, and 14 d (***E***) and 35 d (***F***) post-SCI. Quantification of Lamina I activated cell counts (***G***), and Laminae II+III activated cell counts (***H***). Representative images of DH following ipsilateral forepaw stimulation in laminectomy animals at 14 d (***I***) and 35 d (***J***), and contusion animals at 14 d (***K***) and 35 d (***L***). Quantification of activated neurons in Lamina I (***M***) and in Laminae II+III (***N***). Gray bars in graphs: laminectomy-only; white bars in graphs: cervical contusion. Scale bar: 100 μm.

primary afferents that innervate the forepaw plantar surface (i.e., the peripheral location where we have demonstrated persistent NP-related behavior phenotypes in this cervical contusion SCI mouse model).

We quantified the number of Fos-expressing (activated) neurons in unstimulated mice and found that SCI alone increased DH neuron activation (Fig. 2*C–H*). When we performed this analysis on a per lamina basis, we found that SCI-induced

increases in Fos expression were restricted to Lamina I at both 14 and 35 dpi (ANOVA, $F = 8.53$, $p = 0.004$; Tukey's test: 14d lam. (laminectomy-only) vs 14d cont. (contusion), $p = 0.03$, $n = 4$ mice/group; 35d lam. vs 35d cont., $p = 0.03$, $n = 3$/group; Fig. 2*G*), while there was no difference in neuron activation in deeper laminae of the DH (Laminae II and III; ANOVA, $F = 1.2$, $p = 0.34$; Fig. 2*H*). Importantly, at 14 d postsurgery in laminectomy-only FosTRAP2 mice that did not receive tamoxifen administration, we observed no TdTomato$^+$ cells at all in either the ipsilateral or contralateral cervical DH ($n = 4$ mice; data not shown). Using cFos immunohistochemistry in the DH of mice at 35 dpi (Fig. 3), we found that the changes in FosTRAP2 reporter$^+$ cell counts were accompanied by similar alterations in numbers of cells with cFos protein expression. Specifically, SCI induced an increase in cFos-expressing cells in Lamina I (*t* test, $p = 0.01$, $n = 5$ mice/group; Fig. 3*C*), with no change in Laminae II/III (*t* test, $p = 0.48$, $n = 5$ mice/group; Fig. 3*D*), mirroring our findings in the TRAP2 animals.

Interestingly, we also observed FosTRAP2 reporter$^+$ astrocytes in the spinal cord, based both on morphology (Fig. 3*E*) and co-labeling with GFAP (data not shown). These astrocytes were primarily restricted to the intact, ipsilateral ventral horn caudal to the contusion site (Fig. 3*G*), and were never observed in laminectomy-only animals (Fig. 3*F*; $n = 5$ mice for SCI; $n = 5$ mice for laminectomy; 14 d postsurgery). In addition, we observed occasional Fos$^+$ astrocytes in supraspinal pain locations in a subset of SCI mice, which again was never found in laminectomy-only animals (data not shown).

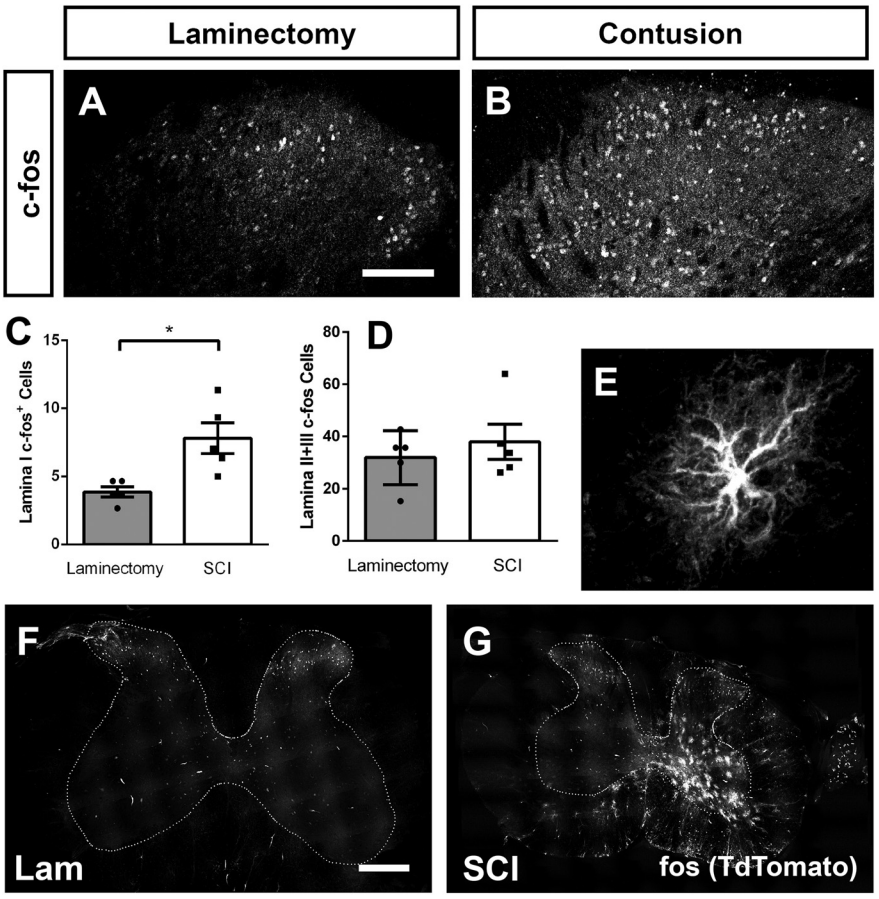

Figure 3. SCI increased the number of c-Fos protein-expressing DH neurons. Immunohistochemistry against c-Fos in the DH 35 d following laminectomy (***A***) or contusion (***B***). Quantification of c-Fos$^+$ cells in Lamina I (***C***), and Laminae II+III (***D***). SCI-induced Fos expression in ventral horn astrocytes: higher-magnification image of a FosTRAP2 reporter$^+$ astrocyte in ipsilateral C7 ventral horn (***E***). Representative transverse section of C7 spinal cord following laminectomy (***F***) or contusion (***G***). Scale bar: 300 μm (***F***, ***G***).

DH neuron activation changes induced by allodynic mechanical stimulation

We next assessed the effect of SCI on DH neuron activation in the context of peripheral sensory stimulation. We chose to assess this in response to mechanical stimulation, as SCI animals in this cervical contusion model develop chronic mechanical allodynia starting one to two weeks postinjury (Heinsinger et al., 2020; Brown et al., 2021). We found a mechanical stimulation induced increase in neuronal activation post-SCI in the DH (Fig. 2*I–N*). When analysis was again stratified by lamina, there was a robust increase in Lamina I neuron activation in SCI animals at both early and late time points (ANOVA, $F = 28.36$, $p < 0.0001$; Tukey's test: 14d lam. vs 14d cont., $p = 0.029$; 35d lam. vs 35d cont., $p < 0.0001$; Fig. 2*M*). Conversely, there was no SCI-induced change in neuron activation in Lamina II/III at 14 or 35 dpi (ANOVA, $F = 1.8$, $p = 0.19$ $n = 3$–6 mice/group; Fig. 2*N*). Furthermore, we mechanically stimulated the plantar surface of the right forepaw of intact FosTRAP2 mice (i.e., animals that received no surgery) with a 1.0-g von Frey filament corresponding to the forepaw withdrawal threshold for uninjured non-SCI mice. When we analyzed FosTRAP2 TdTomato$^+$ labeling in cervical DH in animals stimulated with the 1.0-g filament (Lamina I: 6.083 ± 1.487; $n = 4$; and Laminae II/III: 34.58 ± 3.392; $n = 4$) ipsilateral to the site of forepaw stimulation, we found similar levels of DH neuronal activation between the 1.0- and 0.16-g filament sizes in these laminectomy-only mice.

SCI effects on activation of DH excitatory interneurons

We hypothesized that SCI may differentially affect activation of DH neuronal subtypes, which could consequently alter the excitatory-inhibitory balance of various microcircuits of the DH (e.g., decreased activation of inhibitory interneurons and/or increased activation of excitatory interneurons). To test this, we first quantified TRAP2 reporter labeling in two populations of primarily excitatory DH interneurons with known roles in regulating mechanical nociception. We chose to probe a population located throughout Laminae I and II, characterized by calretinin expression, which has roles in normally regulating DH output in response to cutaneous mechanical stimulation (Petitjean et al., 2019; Smith et al., 2019). After SCI in the absence of mechanical stimulation, there was no SCI-induced change in calretinin$^+$ interneuron activation (ANOVA, $F = 1.92$, $p = 0.17$, $n = 3$–6 mice/group). However, in chronically injured mice presented with mechanical forepaw stimulation, there was a doubling in

the number of activated calretinin$^+$ interneurons (ANOVA, $F = 4.74$, $p = 0.02$; Tukey's test: 35d lam. vs 35d cont., $p = 0.02$, $n = 6$ mice/group; representative images, Fig. 4*A–F*; orthogonal projection of a calretinin$^+$TdTomato$^+$ cell, Fig. 4*G*; quantification in Fig. 4*H*).

The second excitatory interneuron population we assessed expresses PKCγ and is located primarily in the inner band of Lamina II, with small numbers in Lamina III. PKCγ^+ interneurons normally gate non-nociceptive mechanical information, but following peripheral nerve injury, are recruited to pain circuitry, in part because of a loss of inhibitory tone (Neumann et al., 2008; Petitjean et al., 2015). SCI increased PKCγ interneuron activation, which appeared to be mostly stimulation independent (representative images, Fig. 4*I–N*; TdTomato$^+$PKCγ^+ cell orthogonal projection, Fig. 4*O*). PKCγ interneuron activation was increased by SCI at 14d, and mechanical stimulation failed to further activate these neurons (unstimulated: ANOVA, $F = 4.78$, $p = 0.02$; Sidak's: 14d lam. vs cont., $p = 0.03$, 35d lam. vs cont., $p = 0.14$, $n = 3$–6 mice/group; mechanically stimulated: ANOVA, $F = 6.25$, $p = 0.006$; Sidak's: 14d lam. vs cont., $p = 0.02$, $n = 3$ mice/group; 35d lam. vs 35d cont., $p = 0.01$, $n = 6$–7 mice/group; Fig. 4*P*).

Reduced activation of DH inhibitory interneurons after SCI

Given that we found no change in total numbers of activated Laminae II/III neurons post-SCI, but did observe an increase in the activation of two populations of excitatory interneuron subtypes, we hypothesized that there may be a reduced number of activated inhibitory interneurons. To assess this, we first used immunohistochemistry for the transcription factor Pax2, which is necessary for DH inhibitory interneuron differentiation and is expressed by >95% of DH inhibitory interneurons in the adult rodent (Foster et al., 2015; Larsson, 2017). Inhibitory interneurons in Laminae II and III are particularly important for the gating of sensory information; therefore, we restricted our analysis to this region. We first assessed the effect of SCI alone, and found a SCI-induced decrease in Laminae II/III inhibitory neuron activation at both 14 and 35 dpi (ANOVA, $F = 8.61$, $p = 0.0032$. Sidak's: 14d lam. vs 14d cont. $p = 0.05$, $n = 3$ mice/group; 35d lam. vs 35d cont., $p = 0.02$, $n = 3$–6 mice/group; Fig. 5*A–F*; quantification in Fig. 5*G*). Mechanically stimulating the plantar surface of ipsilateral forepaw revealed a further injury dependent decrease in Laminae II/III inhibitory interneuron activation at both acute and chronic time points (ANOVA, $F = 10.16$, $p = 0.0007$; Sidak's: 14d lam. vs 14d cont., $p = 0.0007$, $n = 3$ mice/group; 35d lam. vs 35d cont., $p = 0.01$, $n = 6$–7 mice/group; Fig. 5*H–M*; quantification in Fig. 5*N*). To assess whether the SCI-induced effects on interneuron activation were because of changes in numbers of these interneurons, we quantified interneurons numbers at the same cervical DH location at 35 d post-SCI or laminectomy-only. We found no SCI-induced differences in numbers of Pax2$^+$ cells (t test, $p = 0.77$, $n = 5$ mice; Fig. 6*A*), PKCγ^+ cells (t test, $p = 0.49$, $n = 5$ mice; Fig. 6*B*) or calretinin$^+$ cells (t test, $p = 0.24$, $n = 5$ mice; Fig. 6*C*).

There are several distinct, neurochemically defined populations of inhibitory interneurons in Laminae II/III; therefore, we next sought to determine whether activation of one or more of these subpopulations was differentially reduced by SCI using immunohistochemistry to identify specific markers for each of these subpopulations in chronically injured spinal cord. The first inhibitory subpopulation we assessed was characterized by expression of parvalbumin. These neurons synapse onto excitatory vertical cells and excitatory PKCγ interneurons and play an important role in regulating cutaneous mechanical sensory input (Petitjean et al., 2015). There was no mechanical stimulation induced difference in parvalbumin$^+$ inhibitory neuron activation between SCI and laminectomy animals (Mann–Whitney, $p = 0.64$; Fig. 5*O*). Parvalbumin expressing neurons accounted for 22% of the total activated Laminae II/III inhibitory interneuron population following laminectomy and 33% following contusion. We next assessed NPY expressing Laminae II/III inhibitory interneurons, which make direct projections to Lamina I projection neurons and have a role in transmitting itch, but are not normally in the nociceptive pathway (Iwagaki et al., 2016; Acton et al., 2019). We also found no difference in the number of activated Laminae II/III NPY$^+$ inhibitory interneurons (Mann–Whitney, $p = 0.29$; Fig. 5*P*). This population accounted for 13% of activated Laminae II/III inhibitory interneurons following both SCI and laminectomy. Finally, we assessed activation of Laminae II/III Pax2$^+$ neurons which co-express nNOS$^+$ (Fig. 5*Q*). These cells are directly innervated by primary sensory afferents and synapse directly on Lamina I projection neurons, as well as on PKCγ expressing excitatory neurons in Lamina II (Bernardi et al., 1995; Puskár et al., 2001, Sardella et al., 2011). Activation of these neurons has been shown to suppress mechanical nociception. We found a 56% decrease in total number of activated nNOS$^+$ Pax2$^+$ inhibitory interneurons in SCI compared with laminectomy-only (Mann–Whitney, $p = 0.02$). In laminectomy-only mice, nNOS$^+$ interneurons accounted for 52% of the total number of activated Laminae II/III inhibitory cells, while in SCI animals they accounted for 47% of the total (quantification for all inhibitory interneuron subtypes; Fig. 5*R*, $n = 3$–6 mice/group).

DH neuron activation changes induced by thermal stimulation

Individuals with SCI can experience chronic NP in response to one or multiple sensory modalities (e.g., heat, cold, mechanical; Finnerup et al., 2001; Siddall et al., 2003). Furthermore, DH neuron populations and microcircuits that process this information can vary depending on the sensory modality and can also vary in some cases between normal physiological and nervous system injury conditions (Todd, 2010). For this reason, we examined effects of presenting different forms of sensory stimulation on DH neuron activation changes post-SCI. Specifically, we paired tamoxifen induction with a normally innocuous thermal stimulus (that induces a NP-related behavioral response in cervical contusion mice; Heinsinger et al., 2020; Brown et al., 2021) of the ipsilateral forepaw plantar surface at 35 d after SCI or laminectomy. We then quantified total number of activated neurons at the same DH location as with the mechanical stimulation paradigm. We observed an increase in Lamina I neuron activation in SCI compared with laminectomy in TRAP2 mice, although this effect did not reach statistical significance (t test, $p = 0.06$, $n = 5$ mice/group; Fig. 7*A*,*D*; quantification in Fig. 7*G*). Similar to mechanically stimulated animals, we found no difference in the total numbers of activated Laminae II/III neurons (Mann–Whitney, $p = 0.15$, $n = 5$ mice/group; Fig. 7*H*). As in previous experiments, we next assessed the activation of DH interneuron subpopulations. We first quantified numbers of activated calretinin$^+$ interneurons, as there was a robust increase in their activation in response to mechanical stimulation at 35 dpi. We found that thermal stimulation did not induce an increase in calretinin$^+$ interneuron activation, indicating that at 35 dpi this population may be specifically responding to and transmitting previously innocuous mechanical, but not

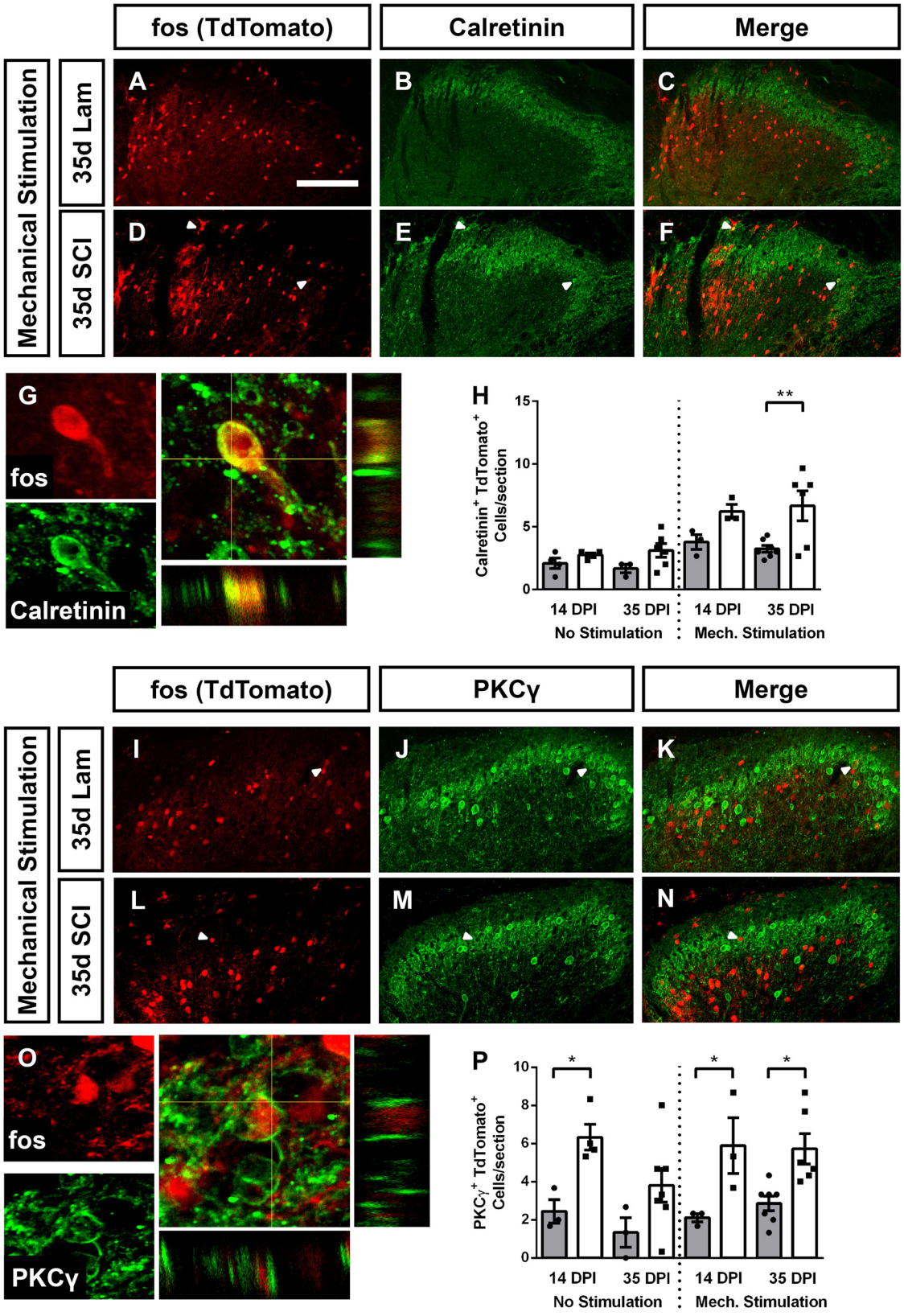

Figure 4. SCI increased activation of excitatory DH interneurons. Cervical SCI increased the activation of calretinin$^+$ DH interneurons following mechanical stimulation of ipsilateral forepaw. Representative DH images of animals that received stimulation 35 d after laminectomy: TdTomato reporter expression (***A***), calretinin expression (***B***), and merged (***C***). Representative DH images of mechanically stimulated animals at 35 d after SCI: reporter expression (***D***), calretinin (***E***), and merged (***F***). High-magnification orthogonal projection of a TdTomato expressing calretinin$^+$ cell (***G***). Quantification of activated calretinin$^+$ neurons (***H***). SCI increased the activation of PKCγ^+ excitatory interneurons both with and without mechanical forepaw stimulation. Representative DH images of mechanically stimulated animals 35 d after laminectomy: TdTomato (***I***), PKCγ (***J***), merge (***K***); and mechanically stimulated animals 35 d post-SCI: TdTomato (***L***), PKCγ (***M***), merge (***N***). High-magnification orthogonal projection of an activated PKCγ^+ interneuron (***O***). Quantification in ***P***. Gray bars in graphs: laminectomy-only; white bars in graphs: cervical contusion. White arrowheads indicate co-labeled cells. Scale bar: 100 μm.

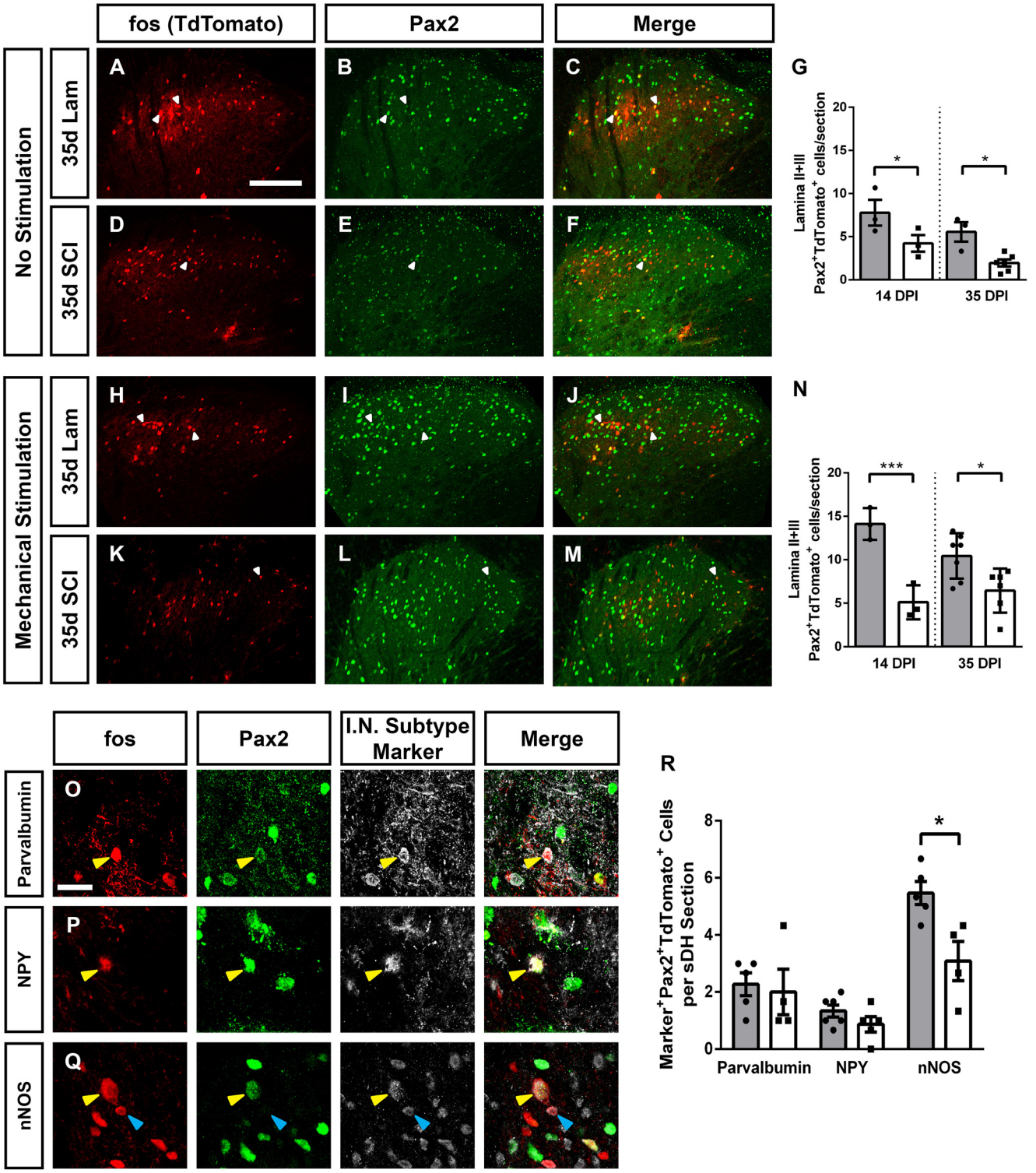

Figure 5. SCI decreased activation of Laminae II/III inhibitory interneurons. SCI alone decreased the activation of Laminae II/III inhibitory interneurons. Representative images of DH without stimulation 35 d following laminectomy: TdTomato (***A***), Pax2 (***B***), and merge (***C***), and following SCI: TdTomato (***D***), Pax2 (***E***), and merge (***F***). Quantification of SCI-induced activation of Laminae II+III Pax2^{+} inhibitory interneurons in the absence of stimulation (***G***). Representative DH images following mechanical stimulation at 35 d after laminectomy: TdTomato (***H***), Pax2 (***I***), and merge (***J***), and 35 d post-SCI: TdTomato (***K***), Pax2 (***L***), and merge (***M***). Quantification of mechanical stimulation induced Pax2^{+} inhibitory interneuron activation (***N***). Representative images of cells triple-labeled for: TdTomato, Pax2, and interneuron subtype-specific marker: parvalbumin (***O***), NPY (***P***), and nNOS (***Q***). Quantification of marker^{+}Pax2^{+}TdTomato^{+} triple-labeled cells 35 d after injury with mechanical stimulation (***R***). Gray bars in graphs: laminectomy-only; white bars in graphs: cervical contusion. White arrowheads indicate double-labeled (in panels ***A–F*** and ***H–M***) or triple-labeled (in panels ***O–Q***) cells; blue arrowheads indicate TdTomato^{+} Pax2^{-} subtype marker^{+} cells. Scale bars: 100 μm (***A***) and 15 μm (***O***).

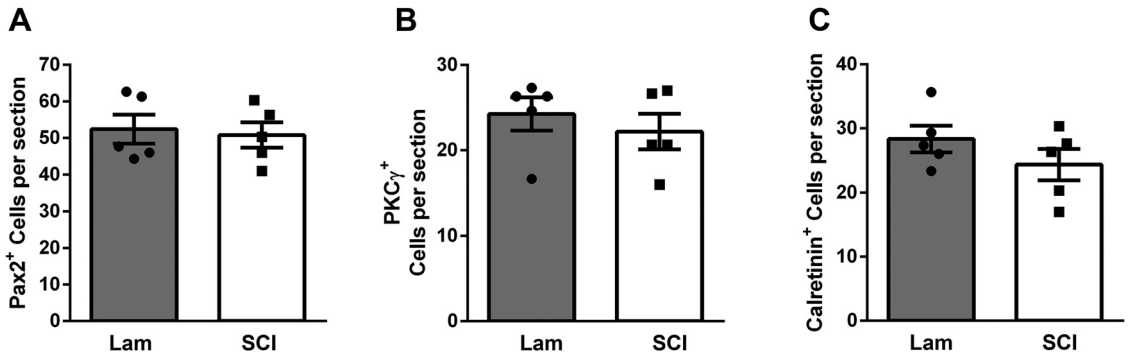

Figure 6. Interneuron numbers were not altered by SCI in the ipsilateral DH caudal to injury. Numbers of neurons expressing Pax2 (***A***), PKCγ (***B***) or calretinin (***C***) were quantified 35 d after laminectomy (white bars) or SCI (gray bars). No significant differences in any population were observed between SCI and laminectomy-only conditions (*t* test, $p > 0.05$).

thermal, sensory information (Mann–Whitney, $p = 0.33$, $n = 5$ mice/group; Fig. 7*A–F*; quantification in Fig. 7*I*). We next assessed SCI-induced changes in activation of Laminae II/III Pax2$^+$ inhibitory interneurons after a thermal stimulus and found a significant decrease in their activation (Fig. 7*K–P*; quantification in Fig. 7*J*; *t* test, 0.006, $n = 3$ mice/group), similar to the mechanical stimulation paradigm. Together, our data indicate that SCI may increase the activation of calretinin$^+$ expressing interneurons in response to mechanical but not thermal stimulation, while possibly causing a multimodality induced reduction in inhibitory interneuron activation.

Cervical SCI did not alter DH neuron activation in lumbar spinal cord

In addition to at-level NP, many individuals affected by SCI experience below-level chronic pain in caudal dermatomes far removed from the anatomic spinal cord level of injury (Finnerup et al., 2001; Siddall et al., 2003). Similar to forepaw NP-related behavioral changes, this cervical contusion mouse model also induces a robust below-level NP-like behavioral phenotype in the form of both mechanical allodynia and thermal hyperalgesia in the hindpaw (Brown et al., 2021). We therefore examined whether cervical SCI altered DH neuron activation in the context of below-level NP by performing TRAP2 analysis in the lumbar L4/5 spinal cord at 14 and 35 d postsurgery. We found no SCI-induced differences between laminectomy-only and SCI mice in activated cell numbers at either time point (ANOVA, $F = 2.66$, $p = 0.07$, $n = 4–7$ mice/group; Fig. 8*A*,*D*; quantification in Fig. 8*G*). We next examined whether, as is the case in the cervical DH, there was a SCI-induced decrease in inhibitory neuron activation. We quantified the number of activated Pax2$^+$ neurons in the L4/L5 DH and found no difference at 35 dpi (Mann–Whitney, $p = 0.51$, $n = 5–6$ mice/group). To further confirm that there was no effect of cervical SCI on inhibitory interneuron activation in the lumbar DH, we next quantified numbers of activated nNOS$^+$ Pax2$^+$ triple-labeled L4/L5 inhibitory interneurons and found no difference in the activation of these cells at 35 dpi (Mann–Whitney, $p = 0.98$, $n = 4–6$ mice/group; Fig. 8*I–L*; quantification in Fig. 8*M*). Taken together, these data suggest that alterations in the excitability of lumbar DH neurons may not be responsible for driving cervical SCI-induced below-level NP.

Increased activation of DH projection neurons

Somatosensory information is transmitted from the periphery, through the DH, and then to various structures in the brain. Lamina I projection neurons are the major ascending conduit for nociceptive sensory information between the spinal DH and supraspinal nuclei. Assessing the effects of SCI on activation of these brain neuron populations is of great importance for understanding how changes in neuron activity across the pain processing neuraxis may be influencing behavior. To assess DH projection neuron activation, we first performed immunohistochemistry for the NK1R specifically in Lamina I. While NK1R does not label all DH projection neurons in the rodent (Choi et al., 2020; Sheahan et al., 2020), it nevertheless does mark a large percentage, particularly in superficial DH (Choi et al., 2020; Sheahan et al., 2020). Furthermore, while a portion of NK1R expressing neurons across the DH are excitatory interneurons, the largest number of these NK1R$^+$ interneurons are present in deeper DH laminae (Sheahan et al., 2020), suggesting that a major portion of the FosTRAP2-labeled NK1R$^+$ cells we quantified in Lamina I are likely projection neurons (especially because we restricted our analysis to NK1R$^+$ cells with a large somal diameter). While analyzing only large somal diameter NK1R$^+$ Lamina I neurons likely increased the proportion of projection neurons included in our quantification, the exact identity of each NK1R$^+$ neuron was unknown. In the absence of mechanical stimulation, SCI alone did not increase the activation of Lamina I NK1R$^+$ neurons (ANOVA, $F = 5.93$, $p = 0.007$, Tukey's test, $p = 0.96$, $n = 3–4$ mice/group; representative images, Fig. 9*A–F*; orthogonal projections of an activated NK1R$^+$ neuron in Fig. 9*G–I*; quantification in Fig. 9*J*). Following mechanical stimulation of the ipsilateral forepaw, however, there was nearly a threefold increase in the number of activated of NK1R$^+$ cells in Lamina I in SCI mice compared with laminectomy-only control (ANOVA, $F = 5.93$, $p = 0.007$; Tukey's test: mechanical stimulation, lam. vs cont., $p = 0.008$, $n = 6$ mice/group).

DH projection neurons synapse in one or more of several supraspinal nuclei that each have distinct roles in pain processing (Todd, 2010). It is important to understand whether SCI differentially alters the activation of subpopulations of DH projection neurons that innervate specific supraspinal locations. To address this question, we paired FosTRAP2 mice with a viral approach to selectively trace the axons of activated DH projection neurons in an anterograde manner from their cell body location in C7/C8 to these supraspinal structures. We intraspinally microinjected an AAV1 vector encoding a Cre-dependent GFP (AAV1-flex-GFP) into the ipsilateral C7 and C8 DH (at two injection sites) at one week before delivering either a C5/6 laminectomy or contusion SCI (Fig. 10*A*, diagram of SCI and intraspinal injection paradigm). At two weeks post-SCI, tamoxifen administration was paired with mechanical stimulation of the ipsilateral forepaw to induce recombination and GFP expression in activated DH

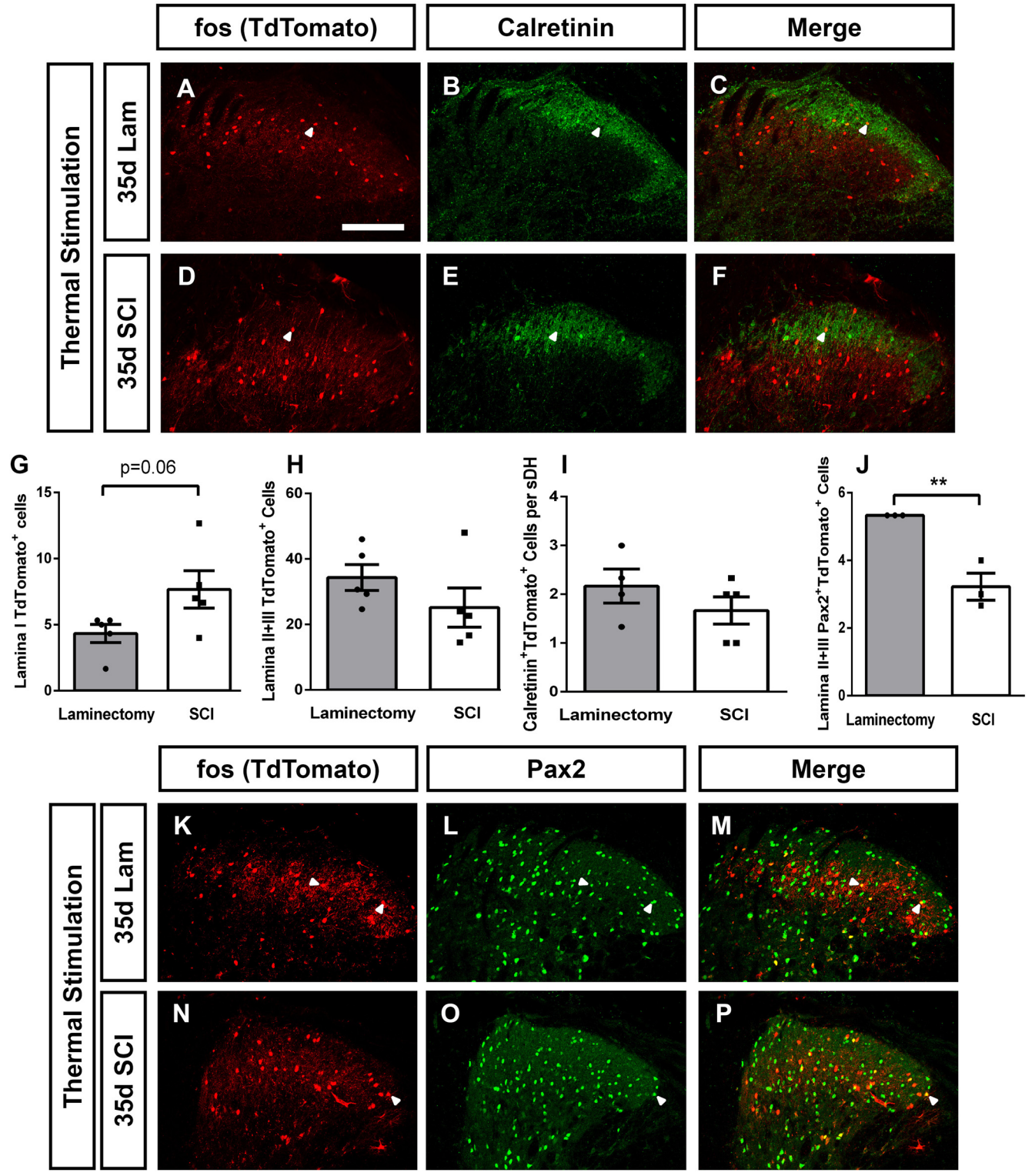

Figure 7. DH neuron activation changes induced by thermal stimulation. Representative DH images 35 d postsurgery following thermal stimulation of the ipsilateral forepaw in laminectomy: TdTomato (***A***), calretinin (***B***), and merge (***C***), and contusion: TdTomato (***D***), calretinin (***E***), and merge (***F***). Quantification of thermal stimulation induced activation of Lamina I cells (***G***), Laminae II+III cells (***H***), activated calretinin^{+} cells (***I***), and activated Laminae II+III Pax2^{+} inhibitory neurons (***J***). Representative ipsilateral DH images 35 d postsurgery following thermal stimulation in the ipsilateral forepaw in laminectomy: TdTomato (***K***), Pax2 (***L***), and merge (***M***), and contusion: TdTomato (***N***), Pax2 (***O***), and merge (***P***). White arrowheads indicate double-labeled cells. Scale bar: 100 μm.

neurons (but only in virus-transduced cells at the site of injection). To ensure adequate time for GFP reporter in axons to anterogradely reach brain structures, animals were killed 10 d posttamoxifen induction (Fig. 10*B*, experimental timeline). Using this paradigm, we were able to efficiently target and restrict viral-delivered reporter expression to the ipsilateral superficial DH (Fig. 10*C*), as well as successfully label anterogradely label anterolateral tract (ALT) axons in the intact contralateral spinal cord

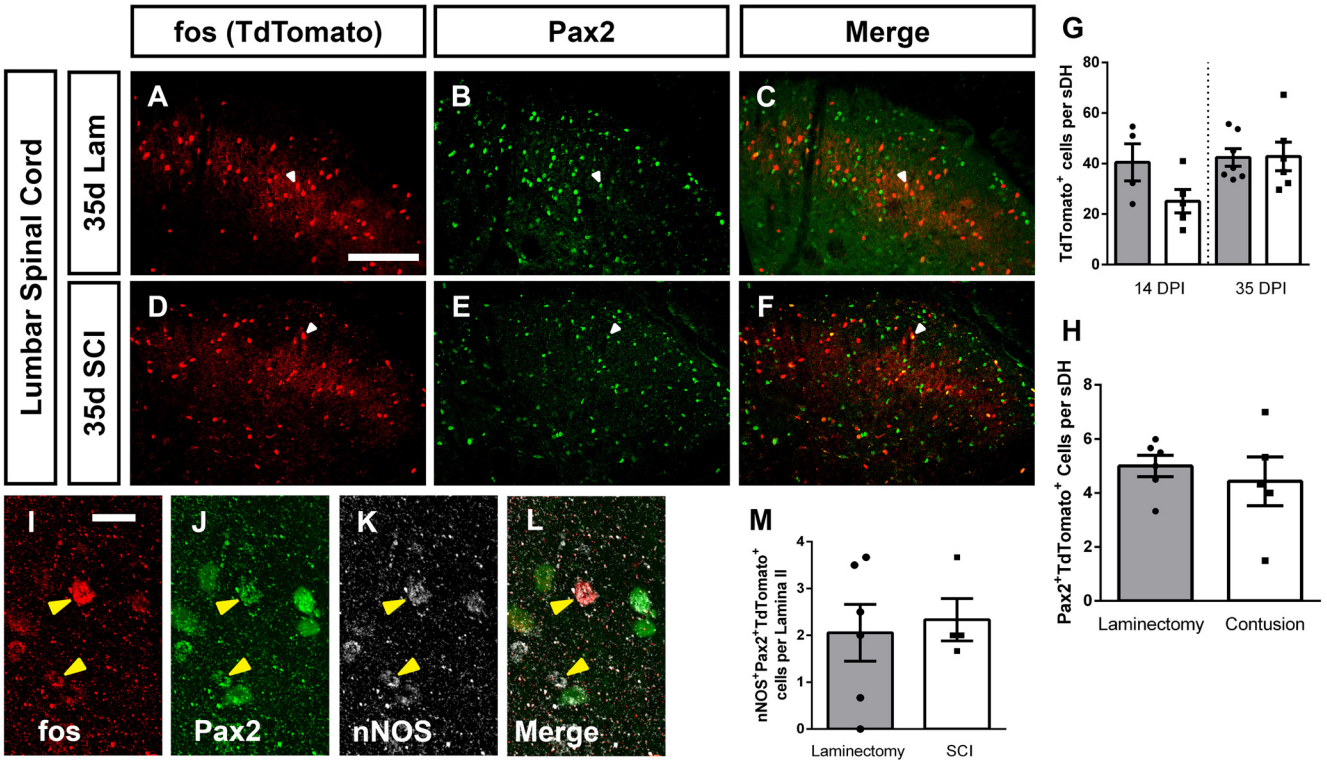

Figure 8. Cervical SCI did not alter DH neuron activation in lumbar spinal cord. Representative DH images from L4/L5 spinal cord 35 d after laminectomy: TdTomato (***A***), Pax2 (***B***), merge (***C***), 35 d postcontusion: TdTomato (***D***), Pax2 (***E***), merge (***F***). Quantification of the number of TdTomato$^+$ (activated) cells per superficial DH section (***G***), and of Tdtomato$^+$Pax2$^+$ cells per superficial DH (***H***). High-magnification representative images of TdTomato$^+$nNOS$^+$Pax2$^+$ triple-labeled cells: TdTomato (***I***), Pax2 (***J***), nNOS (***K***), merge (***L***). Quantification of triple-labeled cells (***M***). Gray bars in graphs: laminectomy-only; white bars in graphs: cervical contusion. White arrowheads indicate double-labeled cells (in panels ***A–F***); yellow arrowheads indicate triple-labeled cells (in panels ***I–L***). Scale bar: 100 μm.

rostral to the contusion site in both SCI and laminectomy animals (Fig. 10*D*,*E*). We quantified numbers of DH projection neuron axons with GFP reporter in the contralateral ALT at a location rostral to the injury site. GFP$^+$ axon density in the contralateral ALT was not significantly different between SCI and laminectomy-only animals (data not shown), suggesting similar degrees of viral transduction of DH projection neurons between the two groups and across all injected mice.

DH projection neurons represent only a small fraction (<5%) of the total neuronal population in Lamina I, and furthermore only a small fraction of ALT neurons project to the thalamus (Spike et al., 2003; Gauriau and Bernard, 2004). In addition, as we chose to only assess activation of DH projection neurons in the small segment of spinal cord most relevant to the at-level pain behavioral phenotype by injecting virus only into C7/8 DH (i.e., the area of DH responsible for processing and transmitting information from forepaw plantar surface), we observed very small numbers of FosTRAP2-labeled GFP$^+$ axon projections in the thalamus (i.e., VPL, VPM, and posterior nucleus). Instead, we focused our analysis on two other nuclei that receive significantly greater amounts of innervation from the spinal cord DH: the LPB and the PAG (Todd, 2010). We first assessed the axon projections of activated cervical DH neurons to the LPB and were able to trace GFP$^+$ axon projections following both SCI and laminectomy-only (Fig. 10*F*,*G*). We quantified both total GFP$^+$ axon profile counts and total GFP$^+$ axon length in the contralateral LPB and did not find a SCI-induced difference in either measure between laminectomy-only and SCI (axon profile count: *t* test, $p = 0.67$; axon profile length: *t* test, $p = 0.71$, $n = 3$–4 mice/group; Fig. 10*H*,*I*). Using the same axon analysis approach, we next quantified the GFP$^+$ axon projections of activated cervical DH neurons to the PAG (Fig. 10*J*–*M*). We found that SCI induced a significant decrease in both total GFP$^+$ axon profile counts and total GFP$^+$ axon length in the PAG (axon profile count: *t* test, $p = 0.01$; axon profile length: *t* test, $p = 0.04$, $n = 5$–6 mice/group; Fig. 10*N*,*O*). These findings suggest there may be a differential effect of SCI on the activation of specific subpopulations of DH projection neurons, depending on where in the brain these cells project, and it is possible that this consequently leads to differential activation of neurons residing in these pain-relevant brain nuclei.

SCI altered neuron activation in pain processing brain regions

To further explore SCI-induced changes in pain circuitry, we again used crossed FosTRAP2 x TdTomato reporter mouse to assess neuronal activation in several relevant brain nuclei. We quantified numbers of activated TdTomato$^+$ cell bodies in the brains of chronically injured mice compared with their laminectomy-only controls (with both groups receiving mechanical stimulation). We restricted our analysis to those brain nuclei that receive ascending spinal projections from DH or those that send descending projections to the DH.

We chose first to quantify neuronal activation in the thalamus, as this is a canonical location most often associated with pain processing. We found a robust SCI-induced increase in the density of activated neurons in contralateral thalamus compared with laminectomy-only (Mann–Whitney, $p = 0.01$, $n = 4$–5 mice/group; Fig. 11*A*, diagram depicting analysis location; representative images in Fig. 11*B*,*C*; quantification in Fig. 11*D*).

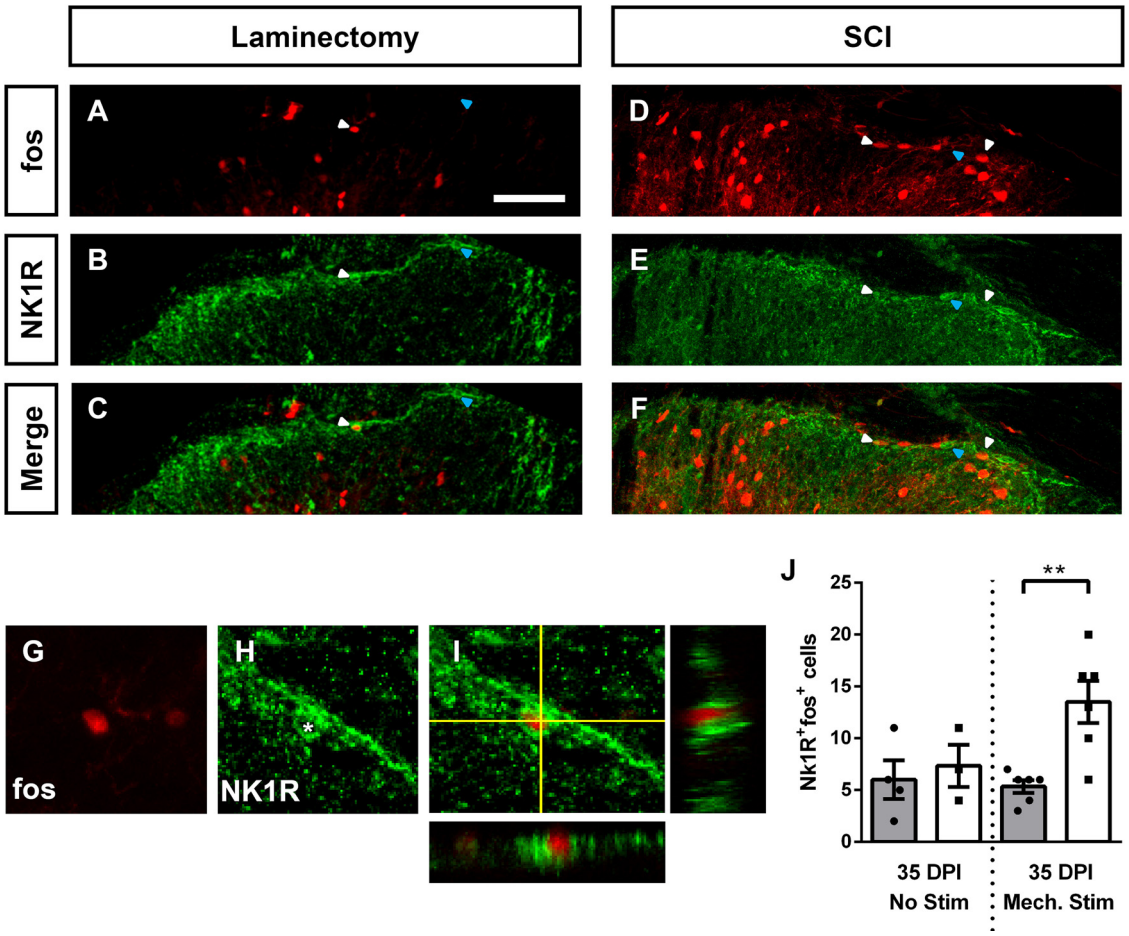

Figure 9. SCI increased activation of DH projection neurons. Representative images of activated Lamina I DH projection neurons following mechanical stimulation at 35 d after laminectomy: TdTomato (***A***), NK1R (***B***), merge (***C***); at 35 d postcontusion: TdTomato (***D***), NK1R (***E***), merge (***F***). Representative high-magnification orthogonal projection of an activated NK1R$^+$ cell: TdTomato (***G***), NK1R (***H***), merge (***I***). Quantification of activated NK1R$^+$ cells in Lamina I (***J***). White arrowheads indicate co-labeled cells; blue arrowheads indicate NK1R$^+$TdTomato$^-$ cells. Gray bars in graphs: laminectomy-only; white bars in graphs: cervical contusion. Scale bar: 70 μm.

We also explored SCI-induced neuron activation changes in brain locations involved in the top-down regulation of DH signaling. Noradrenergic projections from the LC play an important role in the presynaptic modulation of primary sensory afferent and excitatory interneuron signaling in the DH, and dysregulation of each can lead to increased primary afferent signaling and decreased pain thresholds (García-Ramírez et al., 2014). Therefore, we assessed neuronal activation in the LC (Fig. 11*E*, diagram depicting analysis location; representative images in Fig. 11*F*,*G*), but did not find a SCI-induced difference between SCI and laminectomy-only mice (*t* test, $p = 0.45$, $n = 4$-mice/group; Fig. 11*H*).

We next assessed several brainstem and midbrain structures involved in various aspects of pain physiology (Fig. 11*I*, diagram depicting analysis locations; Fig. 11*J*, low-magnification image of brainstem section from FosTRAP2 mouse). We first quantified numbers of activated cells in the LPB and found no difference between SCI and laminectomy-only uninjured animals (*t* test, $p = 0.59$; Fig. 11*K*,*K'*; quantification in Fig. 11*L*). We next quantified neuronal activation in the DR, another region involved descending modulation of DH signaling. Serotonergic fibers originating in the DR innervate DH to modulate pain circuit excitability. We found no SCI-induced effect on neuronal activation in the DR (*t* test, $p = 0.56$; Fig. 11*M*,*M'*; quantification in Fig. 11*N*). Finally, to follow-up on our findings showing decreased innervation of the PAG by activated DH projection neurons after SCI, we quantified numbers of activated neuron cell bodies in the PAG (Fig. 11*O*,*O'*, see also: Fig. 11*K*,*K'*). Interestingly, we observed a significant decrease in the activation of these neurons residing in the PAG in response to cervical SCI (Mann–Whitney, $p = 0.03$, $n = 4$–5 mice/group; Fig. 11*P*). Taken together, these data suggest that SCI may exert differential effects on the activation of neurons in various pain-processing nuclei of the brain.

Discussion

NP is the one of the most common comorbidities of SCI and is often highly debilitating (Finnerup et al., 2001). Due in part to an incomplete understanding of the underlying mechanisms driving this form of chronic pain, it is poorly responsive to current therapeutics (Siddall et al., 2003). Understanding SCI-induced changes in pain circuitry will have important implications for the development of novel therapeutics for this patient population. Here, we have used a clinically relevant model of cervical contusion-type SCI in an activity dependent reporter mouse to describe neuronal activation changes in multiple spinal cord and brain locations critical for pain processing, as well as in specific subpopulations of interneurons and projection neurons of the DH.

Mice injured in our cervical contusion paradigm display several NP-related pain behaviors. These animals develop NP-like

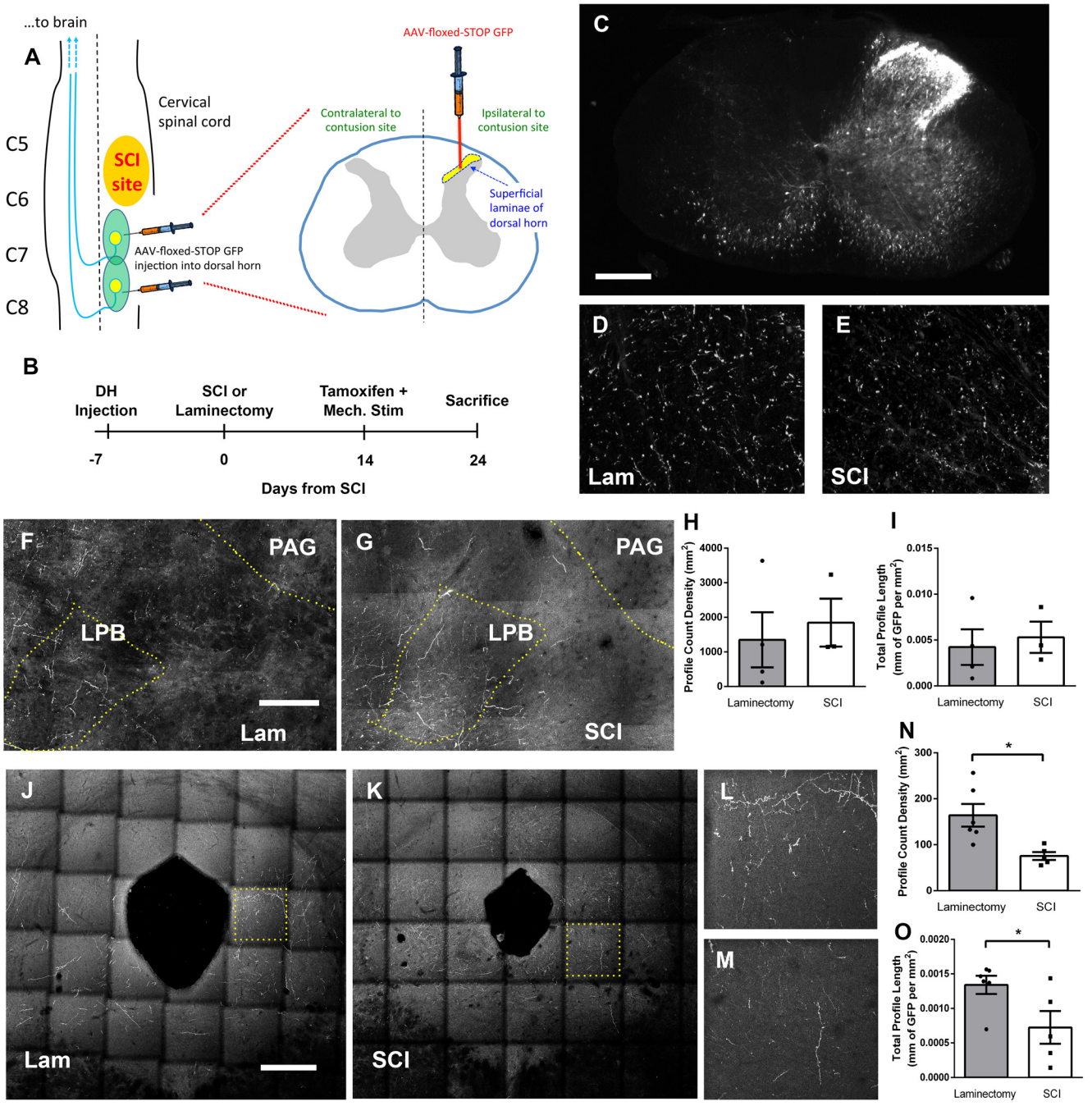

Figure 10. SCI altered activation of DH projection neuron subpopulations. Diagram of intraspinal viral injection experimental paradigm to selectively target ipsilateral DH (***A***). Experimental timeline (***B***). Representative transverse cervical spinal cord section of AAV1-flex-GFP virus injection 10 d post-tamoxifen administration; scale bar: 250 µm (***C***). Representative transverse cervical spinal cord images of FosTRAP2-labeled axons in the contralateral ALT, rostral to the injury site at 10 d post-tamoxifen induction in laminectomy (***D***) or SCI (***E***) animals. Representative coronal images of the LPB following laminectomy (***F***) or SCI (***G***); scale bar: 150 µm. LPB quantification of GFP^+ axon profile counts (***H***) and total GFP^+ axon length (***I***). Representative coronal images of the PAG following laminectomy (***J***) or SCI (***K***); scale bar 375 µm. Higher-magnification insets showing GFP^+ axon fibers in the PAG following laminectomy (***L***) or contusion (***M***). PAG quantification of GFP^+ axon profile counts (***N***) and total GFP^+ axon length (***O***).

hypersensitivity in response to both thermal and mechanical stimuli, both at-level in the forepaw and below-level in the hindpaw (Putatunda et al., 2014; Watson et al., 2014; Ritter et al., 2015; Falnikar et al., 2016; Heinsinger et al., 2020; Brown et al., 2021). In addition, these contusion mice display a spontaneous NP-related phenotype when assessed by facial grimace testing (Heinsinger et al., 2020). We therefore used this SCI model delivered to FosTRAP2 mice to ask questions about how activity of neurons in DH and supraspinal pain processing nuclei is changed after SCI. We were interested in examining how SCI alone may activate this circuitry in the absence of peripheral sensory stimulation, as well as whether pain processing neurons are differentially activated by normally innocuous peripheral stimulation that becomes painful post-SCI.

We found that SCI induced significant reductions in DH inhibitory interneuron activation, increases in DH excitatory interneuron activation, as well as increases in the activation of the DH projection neuron population. Further, our data suggest that SCI induced a selective reduction in activation of DH projection neurons that specifically innervate PAG, as well as decreases in

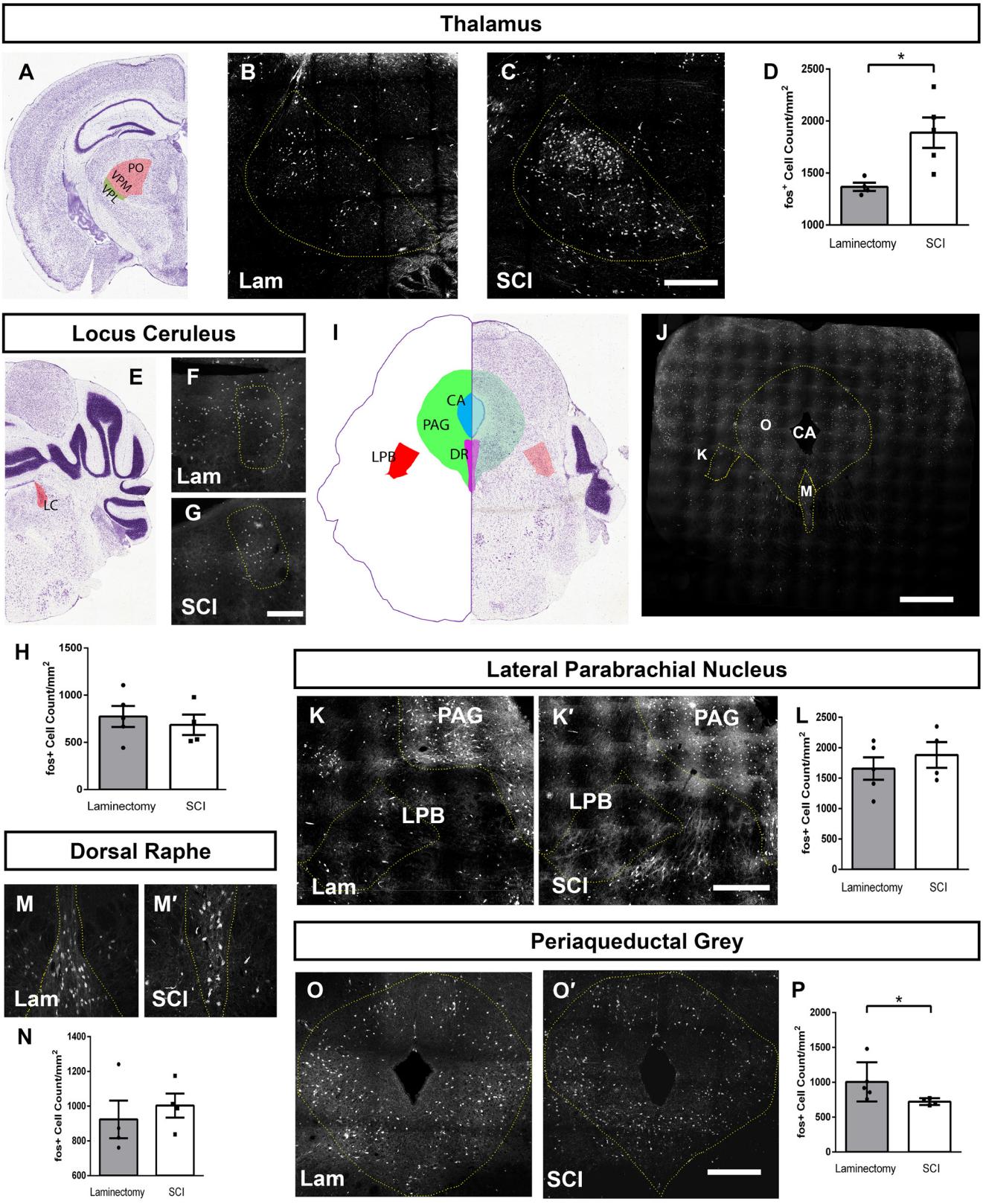

Figure 11. SCI altered neuron activation in pain processing brain regions. Diagram of the location of thalamus quantification (***A***). Representative coronal images of thalamus 35 d after laminectomy (***B***) or contusion (***C***) with mechanical stimulation; scale bar: 350 μm. Quantification of activated cells in thalamus (***D***). Diagram of the location of LC quantification (***E***). Representative coronal LC images following laminectomy (***F***) or contusion (***G***); scale Bar: 150 μm. Quantification of activated LC cells (***H***). Diagram of brainstem cross-section showing locations for quantification of PAG, LPB, and DR. Low magnification of TRAP2 mouse brainstem in cross-section corresponding to diagram in panel ***I*** (***J***); scale bar: 400 μm. Representative coronal images of LPB and PAG following laminectomy (***K***) or contusion (***K′***). Quantification of activated cell counts in LPB (***L***). Representative coronal images of activated cells in DR following laminectomy (***M***) or contusion (***M′***); scale bar: 350 μm. Quantification of activated DR neurons (***N***). Representative coronal images of activated cells in PAG following laminectomy (***O***) or contusion (***O′***); scale bar: 250 μm. Quantification of activated cell counts in PAG (***P***). Image credit for coronal brain images (***A***,***E***,***I***): Allen Institute (2004).

activation of neurons within PAG. We speculate that these changes in PAG-related circuitry may, for example, impact DH signaling via alterations in descending modulation.

We found that SCI induced a decrease in Laminae II/III inhibitory interneuron activation in response to previously innocuous mechanical stimulation specifically in a single interneuron subpopulation characterized by the expression of nNOS. These nNOS interneurons normally make connections with PKCγ^+ excitatory interneurons, as well as with Lamina I projection neurons, and their activation reduces mechanical nociception (Puskár et al., 2001; Sardella et al., 2011; Huang et al., 2018). A decrease in nNOS$^+$ inhibitory interneuron activation, as seen here in response to mechanical stimulation post-SCI, may in part underlie some of the behavioral phenotypes in SCI-induced NP. This could perhaps occur through subsequently increased activation of PKCγ excitatory interneurons and projection neurons, which we also observed following SCI. Future work aimed at specifically increasing the activity of nNOS$^+$ inhibitory interneurons will be important to further define the role of these cells in pain signaling post-SCI.

Previous work in models of peripheral nerve injury has implicated PKCγ interneurons in driving mechanical allodynia. PKCγ interneurons of the DH normally process innocuous, but not noxious, mechanical sensory information (Neumann et al., 2008). Following spared nerve injury, PKCγ neurons lose appositions from inhibitory parvalbumin$^+$ neurons and become recruited into pain circuitry such that normally innocuous mechanical sensory information becomes nocifensive (Petitjean et al., 2015). We find that SCI-induced changes in PKCγ interneuron activation, however, are independent of mechanical stimulation (i.e., occur in both unstimulated and stimulated SCI mice), indicating potentially different mechanisms underlying central versus peripheral nervous system injury mediated chronic pain and highlighting the need for more examination of the role of PKCγ cells in SCI-induced NP.

We also observed mechanical stimulation induced increases in the activation of calretinin-expressing DH interneurons. These cells are primarily located in Laminae I and II and are mostly (80–85%) excitatory, most receive monosynaptic input from TRPV1$^+$ primary afferents, and many synapse specifically with Lamina I spinoparabrachial projection neurons (Smith et al., 2015, 2016; Petitjean et al., 2019). Importantly, they are critical for the passage of mechanical nociceptive information along the spinoparabrachial pathway (Petitjean et al., 2019). We find at 35 d (but not 14 d) after SCI that normally innocuous mechanical stimulation caused activation of calretinin interneurons. Given the LPB's role in regulating aversive and affective responses to pain, this finding has potential implications for understanding SCI-induced anxiety and depression (Petitjean et al., 2019). However, we did not observe changes in LPB neuron activation with SCI. A subpopulation of calretinin-expressing excitatory DH interneurons synapse onto a small subpopulation of DH projection neurons that project to the LPB. Our analysis was unable to probe these two subpopulations specifically; therefore, the observed increase in calretinin neuron activation may be because of other subpopulations of calretinin-expressing DH interneurons that are not presynaptic to LPB-innervating projection neurons. While changes in LPB activation was explored as one possible consequence of altered calretinin neuron activity in the DH, the LPB is not exclusively innervated by DH projection neurons under the control of calretinin interneurons (and the LPB also receives inputs from numerous neuronal populations besides those residing in the DH). Therefore, it is not necessarily surprising that changes in DH calretinin interneuron activation were not accompanied by changes in LPB neuron activation. Future work focused on modulating spinal calretinin neurons (e.g., chemogenetically or optogenetically) could help shed further light on the contribution of calretinin$^+$ interneurons to SCI-induced mechanical allodynia and to their potential contribution to SCI-induced affectual changes (Missig et al., 2017; Sun et al., 2020).

Anterolateral projection neurons form the primary output of DH and are critical to the function of DH and pain circuitry as a whole. They are responsible for carrying peripheral information from DH to supraspinal pain processing nuclei. Understanding how these neurons interact with the neural circuitry of DH and how projection neuron signaling is altered by SCI is critical for understanding the overall pain phenotype. By labeling the DH for the projection neuron marker NK1R, we found that SCI alone was insufficient to alter projection neuron activation. Delivery of a previously innocuous mechanical stimulation, however, caused a robust increase in NK1R neuron activation in contusion mice. This has important implications for defining the mechanisms underlying NP-related behavior in this model. While we have previously reported that mice injured with our cervical contusion SCI paradigm exhibit pain-related behavior in the absence of an external sensory stimulus using facial grimace analysis (Heinsinger et al., 2020), there appeared to be no change in activation of DH projection neurons post-SCI in the absence of allodynic stimulation in the current study. This may suggest that the DH is not involved in driving spontaneous pain behavior post-SCI. It appears that peripheral stimulation is necessary for the activation of DH projection neurons, and loss of input from nNOS$^+$ inhibitory neurons and/or increased input from PKCγ may be necessary for their activation in the context of mechanical allodynia.

As below-level NP also is involved in SCI clinical outcomes, we examined DH neuron activation changes in the lumbar enlargement. Despite observing robust below-level NP phenotypes in the ipsilateral hindpaw similar to those seen in the forepaw (Brown et al., 2021), we previously reported using this cervical contusion model that inflammatory responses involving microglia and macrophage populations observed in cervical superficial DH do not occur in the lumbar superficial DH (Brown et al., 2021). In the present study, we have shown that neuronal activation changes in the cervical DH are also not recapitulated in the lumbar DH after cervical SCI. This may suggest that other alterations, perhaps in supraspinal pain processing nuclei, may play a larger role underlying both spontaneous and below-level NP induced by SCI. We find robust SCI-induced increases in thalamic neuron activation, which has been shown previously via thalamic dysrhythmia to cause persistent, spontaneous pain in patients with complex regional pain syndrome (Walton et al., 2010). It could be that, as just one possible mechanism, dysregulation of the thalamocortical pathway is driving SCI-induced pain behavioral changes under certain conditions.

Given that we observed NP-related behaviors in both the forepaw and hindpaw in this SCI model but did not find increased numbers of FosTRAP2 reporter labeled neurons in the lumbar DH, this raises the question of whether assessment of

activated neurons in the cervical DH using this reporter mouse tool is relevant to the behavior phenotype. In our previous study using this same unilateral cervical contusion mouse model (Watson et al., 2014), we examined levels of a related immediate-early gene, deltaFosB, in neurons of the superficial DH ipsilateral to the cervical contusion site. Similar to the FosTRAP2 reporter in the current study, cervical SCI significantly increased numbers of DH neurons expressing deltaFosB. By restoring expression of the major glutamate transporter GLT1 in cervical DH astrocytes, we were able to reverse already-established NP-related behaviors in the ipsilateral forepaw of these cervical contusion mice. Furthermore, this reversal of the sensory behavioral phenotype was accompanied by a significant reduction in numbers of deltaFosB-expressing cervical DH neurons back to the level observed in control uninjured mice. These findings support the notion that immediate-early gene expression in DH neurons is highly correlated with NP-related behaviors in this cervical SCI model.

We found that the Lamina I neuronal activation response at 35 d in the thermal stimulation paradigm was not as robust as with mechanical stimulation. This cervical contusion mouse model shows consistent NP-related behavioral effects starting 7–14 dpi and persisting for at least six weeks. However, mechanical allodynia is the much more robust phenotype, which is one reason why we chose to make it the main focus of this study. This may in part explain the difference observed in the degree of the DH neuron activation response between these two sensory stimulations. In addition, it is likely that different circuit mechanisms play a role in the development and persistence of thermal versus mechanical hypersensitivity after SCI and other nervous system insults. Along these lines, it is possible that alterations in DH neuron signaling plays a large role in mechanical allodynia than thermal hyperalgesia and that some other location(s) along the pain signaling neuraxis plays a greater involvement in thermal behavior.

While we observed increased activation in the overall population of $NK1R^+$ Lamina I neurons after SCI, we found decreased activation specifically of the subpopulation of projection neurons that innervate PAG. Furthermore, we also uncovered a SCI-induced decrease in activation of neurons that reside in PAG. Given the role of excitatory PAG projections to both DR and LC in regulating the output of these modulatory nuclei (Heinricher et al., 2009), we expected to also find decreased neuronal activation in these two brain locations following SCI, which our data did not show. Changes in expression patterns of noradrenergic and serotenergic receptors in DH have been implicated in driving pain behavioral changes following peripheral nerve injury (Kwon et al., 2014). Therefore, while there was no change in the activation of DR or LC neurons, the involvement of these systems in driving SCI-induced NP cannot be ruled out. Injury induced morphologic changes in descending axons, changes in innervation patterns and/or changes in receptor expression in the DH (to name a few possibilities) may play some role in SCI-induced NP. Future work should aim to determine the contribution, if any, that each of these plays in initiating and maintaining chronic pain after SCI.

In virus-injected mice, we quantified FosTRAP2 reporter expressing axons in the intact, contralateral ALT and found no difference in GFP^+ axon profile density between laminectomy-only and SCI conditions, suggesting there were similar levels of viral transduction of DH projection neurons in both groups. However, quantifying total virus transduction in this experiment presents a challenge, as there is no constitutive transduction reporter as part of our virus system. Instead, only those cells which were transduced and then active at the time of tamoxifen administration were able to be visualized with the GFP reporter. While our GFP^+ axon count data suggest equivalent levels of DH projection neuron transduction across all animals, this experimental consideration should be taken into account when drawing conclusions about the analysis of activated projection neuron axons in Figure 10.

In conclusion, we have demonstrated that the FosTRAP2 reporter mouse is a powerful tool for studying neural circuitry in the context of pathologic pain. We used these mice to show that SCI modulates the activation of a number of important neuron populations in both the DH and brain. In the DH, there are simultaneous SCI-induced increases in activation of excitatory interneurons (both those that express calretinin or PKCγ) and decreases in activation of inhibitory $nNOS^+$ interneurons. In addition, SCI significantly alters the activation of DH projection neurons (including selectively in a specific subpopulation that innervates the PAG), as well as neuron populations residing in pain processing areas of the brain. These findings demonstrate that SCI-induced changes across the pain processing neuraxis are complex and diverse. Future work should aim to understand how SCI drives these divergent changes in activity, with a particular focus on specific subpopulations of DH interneurons and also on PAG-mediated effects such as descending modulation.

References

Acton D, Ren X, Costanzo SD, Dalet A, Bourane S, Bertocchi I, Eva C, Goulding M (2019) Spinal neuropeptide Y1 receptor-expressing neurons form an essential excitatory pathway for mechanical itch. Cell Rep 28:625–639.e6.

Al-Khater KM, Todd AJ (2009) Collateral projections of neurons in laminae I, III, and IV of rat spinal cord to thalamus, periaqueductal gray matter, and lateral parabrachial area. J Comp Neurol 515:629–646.

Allen Institute (2004) Allen mouse brain atlas. Available at https://mouse.brain-map.org/static/atlas.

Bernardi PS, Valtschanoff JG, Weinberg RJ, Schmidt HH, Rustioni A (1995) Synaptic interactions between primary afferent terminals and GABA and nitric oxide-synthesizing neurons in superficial laminae of the rat spinal cord. J Neurosci 15:1363–1371.

Brown EV, Falnikar A, Heinsinger N, Cheng L, Andrews CE, DeMarco M, Lepore AC (2021) Cervical spinal cord injury-induced neuropathic pain in male mice is associated with a persistent pro-inflammatory macrophage/microglial response in the superficial dorsal horn. Exp Neurol 343:113757.

Cameron D, Polgár E, Gutierrez-Mecinas M, Gomez-Lima M, Watanabe M, Todd AJ (2015) The organisation of spinoparabrachial neurons in the mouse. Pain 156:2061–2071.

Cardenas DD, Jensen MP (2006) Treatments for chronic pain in persons with spinal cord. J Spinal Cord Med 29:109–117.

Choi S, Hachisuka J, Brett MA, Magee AR, Omori Y, Iqbal NU, Zhang D, DeLisle MM, Wolfson RL, Bai L, Santiago C, Gong S, Goulding M, Heintz N, Koerber HR, Ross SE, Ginty DD (2020) Parallel ascending spinal pathways for affective touch and pain. Nature 587:258–263.

DeNardo LA, Liu CD, Allen WE, Adams EL, Friedmann D, Fu L, Guenthner CJ, Tessier-Lavigne M, Luo L (2019) Temporal evolution of cortical ensembles promoting remote memory retrieval. Nat Neurosci 22:460–469.

Drew GM, Siddall PJ, Duggan AW (2004) Mechanical allodynia following contusion injury of the rat spinal cord is associated with loss of GABAergic inhibition in the dorsal horn. Pain 109:379–388.

Falnikar A, Hala TJ, Poulsen DJ, Lepore AC (2016) GLT1 overexpression reverses established neuropathic pain-related behavior and attenuates chronic dorsal horn neuron activation following cervical spinal cord injury. Glia 64:396–406.

Finnerup NB, Johannesen IL, Sindrup SH, Bach FW, Jensen TS (2001) Pain and dysesthesia in patients with spinal cord injury: a postal survey. Spinal Cord 39:256–262.

Foster E, Wildner H, Tudeau L, Haueter S, Ralvenius WT, Jegen M, Johannssen H, Hösli L, Haenraets K, Ghanem A, Conzelmann KK, Bösl M, Zeilhofer HU (2015) Targeted ablation, silencing, and activation establish glycinergic dorsal horn neurons as key components of a spinal gate for pain and itch. Neuron 85:1289–1304.

García-Ramírez DL, Calvo JR, Hochman S, Quevedo JN (2014) Serotonin, dopamine and noradrenaline adjust actions of myelinated afferents via modulation of presynaptic inhibition in the mouse spinal cord. PLoS One 9:e89999.

Gauriau C, Bernard JF (2004) A comparative reappraisal of projections from the superficial laminae of the dorsal horn in the rat: the forebrain. J Comp Neurol 468:24–56.

Guenthner CJ, Miyamichi K, Yang HH, Heller HC, Luo L (2013) Permanent genetic access to transiently active neurons via TRAP: targeted recombination in active populations. Neuron 78:773–784.

Gwak YS, Kang J, Unabia GC, Hulsebosch CE (2012) Spatial and temporal activation of spinal glial cells: role of gliopathy in central neuropathic pain following spinal cord injury in rats. Exp Neurol 234:362–372.

Heinricher MM, Tavares I, Leith JL, Lumb BM (2009) Descending control of nociception: specificity, recruitment and plasticity. Brain Res Rev 60:214–225.

Heinsinger NM, Spagnuolo G, Allahyari RV, Galer S, Fox T, Jaffe DA, Thomas SJ, Iacovitti L, Lepore AC (2020) Facial grimace testing as an assay of neuropathic pain-related behavior in a mouse model of cervical spinal cord injury. Exp Neurol 334:113468.

Herschman HR (1991) Primary response genes induced by growth factors and tumor promotors. Annu Rev Biochem 60:281–319.

Huang J, Polgár E, Solinski HJ, Mishra SK, Tseng PY, Iwagaki N, Boyle KA, Dickie AC, Kriegbaum MC, Wildner H, Zeilhofer HU, Watanabe M, Riddell JS, Todd AJ, Hoon MA (2018) Circuit dissection of the role of somatostatin in itch and pain. Nat Neurosci 21:707–716.

Hunt SP, Pini A, Evan G (1987) Induction of c-fos-like protein in spinal cord neurons following sensory stimulation. Nature 328:632–634.

Ibuki T, Hama AT, Wang XT, Pappas GD, Sagen J (1997) Loss of GABA immunoreactivity in the spinal dorsal horn of rats with peripheral nerve injury and promotion of recovery by adrenal medullary grafts. Neuroscience 76:845–858.

Iwagaki N, Ganley RP, Dickie AC, Polgár E, Hughes DI, Del Rio P, Revina Y, Watanabe M, Todd AJ, Riddell JS (2016) A combined electrophysiological and morphological study of neuropeptide Y-expressing inhibitory interneurons in the spinal dorsal horn of the mouse. Pain 157:598–612.

Kami K, Taguchi Ms S, Tajima F, Senba E (2016) Improvements in impaired GABA and GAD65/67 production in the spinal dorsal horn contribute to exercise-induced hypoalgesia in a mouse model of neuropathic pain. Mol Pain 12:174480691662905.

Kwon M, Altin M, Duenas H, Alev L (2014) The role of descending inhibitory pathways on chronic pain modulation and clinical implications. Pain Pract 14:656–667.

Larsson M (2017) Pax2 is persistently expressed by GABAergic neurons throughout the adult rat dorsal horn. Neurosci Lett 638:96–101.

Lepore AC (2011) Intraspinal cell transplantation for targeting cervical ventral horn in amyotrophic lateral sclerosis and traumatic spinal cord injury. J Vis Exp (55):3069.

Lepore AC, O'Donnell J, Bonner JF, Paul C, Miller ME, Rauck B, Kushner RA, Rothstein JD, Fischer I, Maragakis NJ (2011) Spatial and temporal changes in promoter activity of the astrocyte glutamate transporter GLT1 following traumatic spinal cord injury. J Neurosci Res 89:1001–1017.

Li K, Hala TJ, Seetharam S, Poulsen DJ, Wright MC, Lepore AC (2015a) GLT1 overexpression in SOD1(G93A) mouse cervical spinal cord does not preserve diaphragm function or extend disease. Neurobiol Dis 78:12–23.

Li K, Javed E, Hala TJ, Sannie D, Regan KA, Maragakis NJ, Wright MC, Poulsen DJ, Lepore AC (2015b) Transplantation of glial progenitors that overexpress glutamate transporter GLT1 preserves diaphragm function following cervical SCI. Mol Ther 23:533–548.

Mendell LM (2014) Constructing and deconstructing the gate theory of pain. Pain 155:210–216.

Menétrey D, Gannon A, Levine JD, Basbaum AI (1989) Expression of c-fos protein in interneurons and projection neurons of the rat spinal cord in response to noxious somatic, articular, and visceral stimulation. J Comp Neurol 285:177–195.

Missig G, Mei L, Vizzard MA, Braas KM, Waschek JA, Ressler KJ, Hammack SE, May V (2017) Parabrachial pituitary adenylate cyclase-activating polypeptide activation of amygdala endosomal extracellular signal-regulated kinase signaling regulates the emotional component of pain. Biol Psychiatry 81:671–682.

Neumann S, Braz JM, Skinner K, Llewellyn-Smith IJ, Basbaum AI (2008) Innocuous, not noxious, input activates PKCgamma interneurons of the spinal dorsal horn via myelinated afferent fibers. J Neurosci 28:7936–7944.

Petitjean H, Pawlowski SA, Fraine SL, Sharif B, Hamad D, Fatima T, Berg J, Brown CM, Jan LY, Ribeiro-da-Silva A, Braz JM, Basbaum AI, Sharif-Naeini R (2015) Dorsal horn parvalbumin neurons are gate-keepers of touch-evoked pain after nerve injury. Cell Rep 13:1246–1257.

Petitjean H, Bourojeni FB, Tsao D, Davidova A, Sotocinal SG, Mogil JS, Kania A, Sharif-Naeini R (2019) Recruitment of spinoparabrachial neurons by dorsal horn calretinin neurons. Cell Rep 28:1429–1438.e4.

Polgár E, Hughes DI, Arham AZ, Todd AJ (2005) Loss of neurons from laminas I-III of the spinal dorsal horn is not required for development of tactile allodynia in the spared nerve injury model of neuropathic pain. J Neurosci 25:6658–6666.

Polgár E, Al Ghamdi KS, Todd AJ (2010a) Two populations of neurokinin 1 receptor-expressing projection neurons in lamina I of the rat spinal cord that differ in AMPA receptor subunit composition and density of excitatory synaptic input. Neuroscience 167:1192–1204.

Polgár E, Wright LL, Todd AJ (2010b) A quantitative study of brainstem projections from lamina I neurons in the cervical and lumbar enlargement of the rat. Brain Res 1308:58–67.

Polgár E, Sardella TCP, Tiong SYX, Locke S, Watanabe M, Todd AJ (2013) Functional differences between neurochemically defined populations of inhibitory interneurons in the rat spinal dorsal horn. Pain 154:2606–2615.

Puskár Z, Polgár E, Todd AJ (2001) A population of large lamina I projection neurons with selective inhibitory input in rat spinal cord. Neuroscience 102:167–176.

Putatunda R, Hala TJ, Chin J, Lepore AC (2014) Chronic at-level thermal hyperalgesia following rat cervical contusion spinal cord injury is accompanied by neuronal and astrocyte activation and loss of the astrocyte glutamate transporter, GLT1, in superficial dorsal horn. Brain Res 1581:64–79.

Ritter DM, Zemel BM, Hala TJ, O'Leary ME, Lepore AC, Covarrubias M (2015) Dysregulation of Kv3.4 channels in dorsal root ganglia following spinal cord injury. J Neurosci 35:1260–1273.

Sardella TC, Polgár E, Watanabe M, Todd AJ (2011) A quantitative study of neuronal nitric oxide synthase expression in laminae I-III of the rat spinal dorsal horn. Neuroscience 192:708–720.

Sheahan TD, Warwick CA, Fanien LG, Ross SE (2020) The neurokinin-1 receptor is expressed with gastrin-releasing peptide receptor in spinal interneurons and modulates itch. J Neurosci 40:8816–8830.

Siddall PJ, McClelland JM, Rutkowski SB, Cousins MJ (2003) A longitudinal study of the prevalence and characteristics of pain in the first 5 years following spinal cord injury. Pain 103:249–257.

Smith KM, Boyle KA, Madden JF, Dickinson SA, Jobling P, Callister RJ, Hughes DI, Graham BA (2015) Functional heterogeneity of calretinin-expressing neurons in the mouse superficial dorsal horn: implications for spinal pain processing. J Physiol 593:4319–4339.

Smith KM, Boyle KA, Mustapa M, Jobling P, Callister RJ, Hughes DI, Graham BA (2016) Distinct forms of synaptic inhibition and neuromodulation regulate calretinin-positive neuron excitability in the spinal cord dorsal horn. Neuroscience 326:10–21.

Smith KM, Browne TJ, Davis OC, Coyle A, Boyle KA, Watanabe M, Dickinson SA, Iredale JA, Gradwell MA, Jobling P, Callister RJ, Dayas CV, Hughes DI, Graham BA (2019) Calretinin positive neurons form an excitatory amplifier network in the spinal cord dorsal horn. Elife 8:e49190.

Spike RC, Puskár Z, Andrew D, Todd AJ (2003) A quantitative and morphological study of projection neurons in lamina I of the rat lumbar spinal cord. Eur J Neurosci 18:2433–2448.

Sun L, Liu R, Guo F, Wen MQ, Ma XL, Li KY, Sun H, Xu CL, Li YY, Wu MY, Zhu ZG, Li XJ, Yu YQ, Chen Z, Li XY, Duan S (2020) Parabrachial nucleus circuit governs neuropathic pain-like behavior. Nat Commun 11:5974.

Tashima R, Koga K, Yoshikawa Y, Sekine M, Watanabe M, Tozaki-Saitoh H, Furue H, Yasaka T, Tsuda M (2021) A subset of spinal dorsal horn interneurons crucial for gating touch-evoked pain-like behavior. Proc Natl Acad Sci U S A 118:e2021220118.

Todd AJ (2010) Neuronal circuitry for pain processing in the dorsal horn. Nat Rev Neurosci 11:823–836.

Todd AJ (2017) Identifying functional populations among the interneurons in laminae I-III of the spinal dorsal horn. Mol Pain 13:1744806917693003.

Walton KD, Dubois M, Llinás RR (2010) Abnormal thalamocortical activity in patients with complex regional pain syndrome (CRPS) type I. Pain 150:41–51.

Watson CG, Paxinos G, Kayalioglu C Heise (2009) Atlas of the mouse spinal cord. In: The spinal cord, Chapter 16 (WatsonC, Paxinos G, and KayaliogluG, eds), pp 308–379. San Diego: Academic Press.

Watson JL, Hala TJ, Putatunda R, Sannie D, Lepore AC (2014) Persistent at-level thermal hyperalgesia and tactile allodynia accompany chronic neuronal and astrocyte activation in superficial dorsal horn following mouse cervical contusion spinal cord injury. PLoS One 9:e109099.

Wercberger R, Basbaum AI (2019) Spinal cord projection neurons: a superficial, and also deep, analysis. Curr Opin Physiol 11:109–115.